Bioorganic Chemistry 85 (2019) 455–468

Contents lists available at ScienceDirect

Bioorganic Chemistry

journal homepage: www.elsevier.com/locate/bioorg

Novel lawsone-containing ruthenium(II) complexes: Synthesis, characterization and anticancer activity on 2D and 3D spheroid models of prostate cancer cells

Rone Aparecido De Grandis[a,*], Patrick Wellington da Silva dos Santos[b], Katia Mara de Oliveira[c], Ana Rita Tomazela Machado[b], Alexandre Ferro Aissa[b], Alzir Azevedo Batista[c], Lusânia Maria Greggi Antunes[b], Fernando Rogério Pavan[a,*]

[a] School of Pharmaceutical Sciences, São Paulo State University, Araraquara, São Paulo 14800-903, Brazil
[b] School of Pharmaceutical Sciences of Ribeirão Preto, University of São Paulo, Ribeirão Preto, São Paulo 14040-903, Brazil
[c] Department of Chemistry, Federal University of São Carlos, São Carlos, São Paulo 13561-901, Brazil

ARTICLE INFO

Keywords:
Cancer
1,4-naphthoquinone
3D-cell culture
ROS
Apoptosis
BAX/BCL-2

ABSTRACT

This study describes a series of newly synthesized phosphine/diimine ruthenium complexes containing the lawsone as bioligand with enhanced cytotoxicity against different cancer cells, and apoptosis induction in prostatic cancer cells DU-145. The complexes $[Ru(law)(N\text{-}N)_2]PF_6$ where N-N is 2,2′-bipyridine (**1**) or 1,10-phenanthroline (**2**) and $[Ru(law)(dppm)(N\text{-}N)]PF_6$, where dppm means *bis*(diphenylphosphino)methane, N-N is 2,2′-bipyridine (**3**) or 1,10-phenanthroline (**4**), and law is lawsone, were synthesized and fully characterized by elemental analysis, molar conductivity, NMR, UV–vis, IR spectroscopies and cyclic voltammetry. The interaction of the complexes (**1**–**4**) with DNA was evaluated by circular dichroism, gel electrophoresis, and fluorescence, and the complexes presented interactions by the minor grooves DNA. The phosphinic series of complexes exhibited a remarkably broad spectrum of anticancer activity with approximately 34-fold higher than cisplatin and 5-fold higher than doxorubicin, inhibiting the growth of 3D tumor spheroids and the ability to retain the colony survival of DU-145 cells. Also, the complex (**4**) inhibits DU-145 cell adhesion and migration potential indicating antimetastatic properties. The mechanism of its anticancer activity was found to be related to increased reactive oxygen species (ROS) generation, increased the *BAX/BCL-2* ratio and subsequent apoptosis induction. Overall, these findings suggested that the complex (**4**) could be a promising candidate for further evaluation as a chemotherapeutic agent in the prostate cancer treatment.

1. Introduction

The research based on transition metals was strongly encouraged thanks to the quest for novel anticancer therapies [1]. So far, cisplatin is probably still the most essential chemotherapeutic based on metals complexes. However, platinum complexes have caused several side effects and cross drug resistance which limited their applications [2]. Therefore, the development of novel metallodrugs agents remains a significant challenge.

In this important field, ruthenium-based complexes are highlighted due to its unique properties as chemical stability, a variety of oxidation states, structural diversity, low toxicity and ability to mimic iron binding in the biological system [3–6]. Moreover, several ruthenium (Ru) complexes have been foreground reported due to its antimetastatic activities, low toxicity to non-cancer cells and high selectivity for tumor cells [7,8]. For instance, some Ru complexes as NAMI-A (*trans*-$[RuCl_4(1H\text{-imidazole})(DMSO\text{-}S)]$), NKP-1339 (sodium [*trans*-$RuCl_4(1H\text{-indazole})_2$]) and KP1019 (*trans*-$[RuCl_4(1H\text{-in-dazole})_2]$) have been evaluated in preclinical and phase I or II clinical trials, representing a novel class of less toxic antineoplastic chemotherapy [9,10]. Accumulative evidences suggest that Ru-based compounds could act as potential anticancer agents through molecular mechanisms providing an increase of reactive oxygen species (ROS) [11], DNA intercalation [12], DNA damage [13], induction of cell apoptosis and metastasis inhibition [14,15].

One rational approach to improve the efficacy of metal complexes consists of incorporating different chelating ligands with complementary biological activity to enhance the physiological targets of

* Corresponding authors.
E-mail addresses: degrandis.rone@fcfar.unesp.br (R.A. De Grandis), fernando.pavan@unesp.br (F.R. Pavan).

https://doi.org/10.1016/j.bioorg.2019.02.010
Received 11 September 2018; Received in revised form 29 January 2019; Accepted 3 February 2019
Available online 08 February 2019
0045-2068/

the metallodrug. In this context, active ligands with quinone moiety represent an unquestioned tool in bioinorganic medicinal chemistry for improving the anticancer activity of metal complexes. Undoubtedly, some quinone based drugs such as doxorubicin, mitomycin C, and mitoxantrone are recognized as FDA-approved compounds with excellent anticancer properties [16,17]. A representative class of quinone compounds, known as naphthoquinones, widely distributed in nature, have been recognized to own an extensive range of biological activities such as antimicrobial [18], antiparasitic [19], antiviral [20] and anticancer activity [21].

Mainly, 1,4-naphthoquinone, or lawsone, is an example of a natural compound that contains two ketone groups as suitable chromophore responsible for its biological activity due to their ability to accept electrons [22,23]. Recently, lawsone compounds have shown promising pharmacological effects presenting antiproliferative activity in a large number of cancer cell lines and inhibition of tumor burden *in vivo* [24,25].

Furthermore, findings indicated that anticancer activity also might be related to the inhibition of the enzyme DNA-topoisomerase II [26]. Lawsone can bind potentially to metal ions in different oxidations states coordinating metals in a bidentate way which allows them to play an essential role in biological systems [27]. Indeed, some metal complexes containing lawsone ligands have been exhibited higher biological activity than free lawsone [28]. Therefore, as part of our ongoing effort to design multi-target bioactive metallodrug candidates, in the last years our research group has synthesized several Ru-complexes containing phosphine and diimines ligands with promising pharmacological activities for anticancer proposes [29–35]. In light of these considerations and of some previous results, herein we have investigated the anticancer properties of the newly synthesized phosphine/diimine Ru-complexes containing lawsone as bioligand. The corresponding complexes **1–4** (showed in Fig. 1) were synthesized and characterized, and their potential as anticancer agents was investigated for the first time towards a comprehensive panel of human cancer cell lines cultured in conventional and 3D models. Besides, we analyzed the antimetastatic effects on human prostate carcinoma DU-145 cells and their ability to interact with CT-DNA. Finally, for elucidating the anti-cancer functions and molecular mechanisms, reactive oxygen species (ROS) production and apoptosis-inducing ability were also investigated.

2. Results and discussion

2.1. Synthesis of novel lawsone-containing ruthenium complexes

The complexes (**1–4**) containing lawsone (law), phosphines and diimines as ligands were obtained according to the procedure illustrated in Fig. 1.

The synthetic route obtained pure complexes with high-yield according to spectroscopic data, as well as elemental analyses, molar conductivity and 31P{1H}, 1H and 13C NMR spectrum. All complexes are dark purple air-stable solids, soluble in dichloromethane, acetone, methanol, dimethyl sulfoxide and water insoluble.

In the IR spectra of the free law is observed the intense band of the stretching modes of the phenolic ν(O–H) around 3200 cm^{-1}, this band disappear from the spectra of all complexes, indicating the ligand deprotonation and the coordination by oxygen. The band relative to the carbonyl group (C_1=O) at 1640 cm^{-1} in the free law were shifted to lower frequencies, around 1603 cm^{-1} in the complexes, denoting the bidentate coordination. Also, the band at 1679 cm^{-1} of the group (C_4=O) also presented a small displacement to lower frequencies, 1614 cm^{-1}. The band C_2–O presented displacement from 982 cm^{-1} to 1098 cm^{-1}, approximately, in the complexes, which are in concordance with the coordination by the oxygen. The same behavior was observed for others ruthenium complexes containing the lawsone as ligand [28].

The complexes (**1–4**) were characterized by $^{31}P\{1H\}$, ^{1}H and ^{13}C NMR spectroscopy. In the $^{31}P\{1H\}$ of complexes (**3**) and (**4**) was

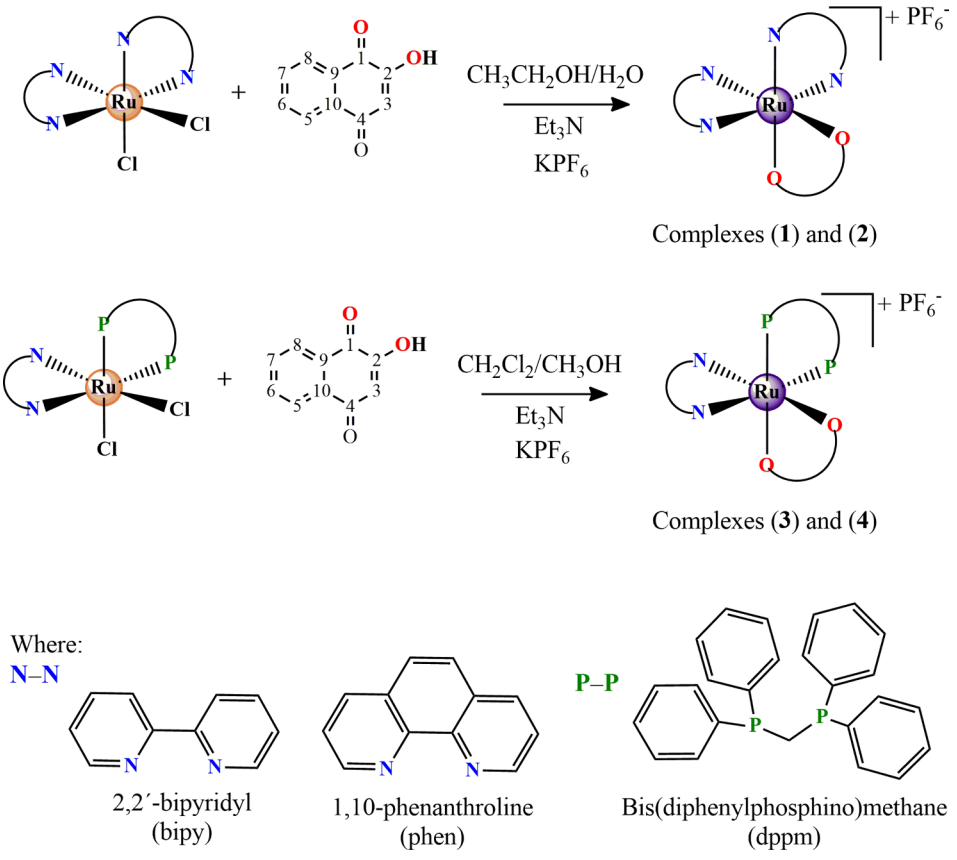

Fig. 1. Synthetic route to the preparation of the new ruthenium complexes containing the naphthoquinone lawsone.

observed four pairs of signals (17.9/6.7 ppm and 15.2/5.9 ppm for complex (**3**) and 18.2/6.6 ppm and 15.4/6.2 ppm for complex (**4**)) for the two phosphorus atoms of biphosphine dppm, indicating the non-equivalence of phosphorus. The duplication of the signals is due to the formation of isomers, where there is an isomer with the phosphorus atom of dppm trans to the oxygen of the carbonyl of lawsone, and in the other, the oxygen atom of the carbonyl is trans to the nitrogen of bipy or phen (see Supplementary Information, Figs. S2–S3). In the ^{1}H spectra of all complexes were observed the presence of the singlet at ca. 5.8 ppm belonging to the hydrogen of bonded to carbon 3 of lawsone. In the case of complex (**4**) was observed in the region of 9.2–6.3 multiplets referring to 32 hydrogen atoms from the dppm, phen and law, and in 5.5 ppm was observed the multiplet attributed to the CH_2 of aliphatic chain of dppm. All complexes presented the same behavior.

Characteristic NMR ^{13}C signals belonging to the carbon of carbonyl groups of lawsone were observed for complex (**4**) at 200.3 ppm (C_1═O), 182.5 ppm (C4═O) and 172.6 ppm (C_2−O). These signals are observed in 184.5 ppm (C_1═O), 181.2 ppm (C4═O) and 159.5 ppm (C_2−O) in free lawsone. The most significant displacements are found for the carbons atoms of the groups C_1═O and C_2−O, indicating the coordination of these oxygen atoms. More recently, our research group developed *trans*-[Ru(law)(PPh_3)$_2$(N-N)]PF_6 complexes and were observed the same behavior in NMR experiments [31].

The electrochemical behavior of the complexes was evaluated by cyclic voltammetry and the redox process Ru(II)/Ru(III) for all complexes were observed in the region of 1–1.1 V. The values are higher than those for complexes precursors, which occur around 0.1–0.6 V. This difference can be explained by the higher stability of the complexes after coordination of lawsone, due the replacement of two chlorides σ and π donor by a negative monocharged chelating lawsone.

2.2. Partition coefficient (log P) study

Determining the lipophilicity is an important physicochemical property that figures out the possible pharmacokinetic and pharmacodynamic profile of new drugs candidates in the discovery development phase [36]. The well-known shake-flask has been widely recommended as a reference method to determine a partition coefficient experimentally [37]. The log *P*(o/w) values, calculated by the shake-flask method, were positive and ranged from 0.228 ± 0.012 to complex (**1**), 0.573 ± 0.023 to complex (**2**), 0.437 ± 0.025 to complex (**3**) and 0.793 ± 0.031 to complex (**4**). As demonstrates, the higher lipophilicity of complexes (**2**) and (**4**) can be attributed to the presence of phen ligand. Other studies established that the presence of 1,10-Phenanthroline acts improving the lipophilicity of silver complexes when compared to bipyridine analogs [38]. Our finding also suggests that the use of diphosphines as ligands can adjust the lipophilic/hydrophilic balance in metal complexes, where in general, its biological activity is found to increase thanks to an increase in the lipophilicity [39]. Thus, the log *P* indicates that the coordination of phen and dppm chelating ligands in one single molecular structure improve the lipophilicity and, as a consequence, may contribute to enhance the cell membrane permeability and its biological activity.

2.3. The complexes display enhanced cytotoxicity against a panel of cancer cell lines

The cytotoxicity of the ruthenium complexes was evaluated in a panel of different histological types of cancer cell lines (A549, Caco-2, DU-145, HepG2, PC-3 and MDA-MB-231) and against two non-cancer cells (FGH and HUVEC) in two-dimensional (2D) culture by Alamar Blue assay 24 h after incubation, as shown in Table 1. All of the complexes presented enhanced cytotoxicity to different cancer cells and more potent activity than metal-free lawsone. The synthesized Ru(II) phosphine complexes investigated exhibited remarkable cytotoxic properties displaying better anticancer activity than cisplatin (Fauldcispla®) and doxorubicin (Fauldoxo®). As expected, the phosphine-coordinating ligand improved not only the lipophilicity of ruthenium compounds but also their biological activity. Metal complexes with different phosphine ligands had antitumor profiles characterized by high cytotoxic potency and selectivity between different cancer cells [40,41]. Compared to the other complexes and metal-free lawsone, the phosphine complexes (**3**) and (**4**) had low IC_{50} values, where complex (3) presented IC_{50} values ranging from to 1.9 to 4.8 μM for cancer cell lines DU-145 and A549, respectively and (**4**) presented IC_{50} values ranging from 1.3 to 3.0 μM for cancer cell lines DU-145 and MDA-MB-231, respectively.

In addition, complex (**3**) was more potent than cisplatin in A549 (3-fold), Caco-2 (7-fold), DU-145 (12-fold), HepG2 (6-fold), PC-3 (6-fold) and MDA-MB-231 (10-fold). Complex (**4**) was more potent than doxorubicin on DU-145 (4-fold), HepG2 (2-fold), PC-3 (2-fold) and cisplatin on A549 (4-fold), Caco-2 (8-fold), DU-145 (18-fold), HepG2 (6-fold), PC-3 (9-fold) and MDA-MB-231 (12-fold). The precursors of types [$RuCl_2$(N-N)$_2$]PF_6) and [$RuCl_2$(dppm)(N-N)]PF_6 (N-N = 2,2′-bipyridine or 1,10-phenanthroline) exhibited weak cytotoxicity (IC_{50} > 100 μM). The IC_{50} value for non-cancer cells was 4.3 and 8.1 μM for the complex (**3**), 3.2 and 6.9 μM for the complex (**4**) and 1.9 and 4.6 μM for doxorubicin on FGH and HUVEC cells, respectively.

Table 2 shows the calculated selectivity index (SI) of each compound. The SI was calculated using the following formula: SI = IC_{50} [non-cancer cells]/IC_{50} [cancer cells]. The SI is a clear manner to estimate the therapeutic range of a drug and to identify drug candidates for further studies [11]. Complexes (**3**) and (**4**) were more cytotoxic and selective to prostate cancer cells DU-145. Furthermore, both complexes exhibit selectivity index greater than displayed by the drug controls cisplatin and doxorubicin, which are clinically useful drugs in the treatment of cancer. Probably, the presence of the dppm ligand in the complexes (**3**) and (**4**) may contribute to increasing cytotoxic activity, as previously observed for other ruthenium complexes, where the increase of phosphine ligands is directly related to the increase of biological activity [30,42].

The promising cytotoxic activity of the complexes (**3**) and (**4**) towards prostate cancer cells encouraged us to study their effects at the cellular level. In a new set of experiment, DU-145 cell line was used as a cellular model, since it was among the most sensitive cell line to the complexes tested. Therefore, the cytotoxicity of phosphine complexes was confirmed by clonogenic survival assay that is extremely sensitive to determine the effects on cell proliferation after treatments. Clonogenic assays represent the gold-standard method to study the cytotoxic and constitute a traditional technique of choice to determine the long-term effect of proliferating cells [43]. The results revealed that both complexes inhibited cell colony formation of DU-145 cells in a dose-dependent manner as shown in Fig. 2A. The plating efficiency of untreated DU-145 cells was higher than 70% for all replicates. Moreover, following seven days of culture, the inhibitory effect of the complex (**4**) was greater than that of the complex (**3**) at the same concentration. At concentrations of 0.125, 0.25, 0.5 and 1 μM, the complex (**3**) reduced the colony-forming presenting survival fractions (SF) of 79.1, 68.2, 31.1 and 13.4%, respectively. Complex (**4**), at same concentrations, presented SF of 68.1, 39.5, 22.4 and 5.1%, respectively. No significant (p > 0.05) decrease in the number of colonies was observed in control (DMSO 0.1% v/v). Few colonies of DU-145 cells were visible after incubation with 1 μM of (**4**) which indicates that the substitution of diimine ligand increases the activity of the compound (Fig. 2B).

The higher cytotoxicity, exhibited by complexes (**3**) and (**4**), indicated that the coordination of phosphine and lawsone chelating ligands in one single molecule made it possible to create a compound with increased antitumor activity. Furthermore, these findings predicted the loss of clonogenicity of DU-145 cells after the exposure with (**3**) and (**4**) which is an effective parameter to distinguish the cytostatic of the cytotoxic effects of drug treatments [44]. Cisplatin did not

Table 1
Cytotoxic activity of Ru complexes in human cell lines.

	IC_{50} in μM							
	FGH	HUVEC	A549	Caco-2	DU-145	HepG2	PC-3	MDA-MB-231
BB	> 100	> 100	> 100	> 100	> 100	> 100	> 100	> 100
BP	> 100	> 100	> 100	> 100	> 100	> 100	> 100	> 100
DB	> 100	> 100	> 100	> 100	> 100	> 100	> 100	> 100
DP	> 100	> 100	> 100	> 100	> 100	> 100	> 100	> 100
LAW	> 100	> 100	> 100	> 100	> 100	> 100	> 100	> 100
(1)	74.3 ± 1.4	93.1 ± 7.4	99.1 ± 0.2	60.3 ± 5.3	41.4 ± 4.5	53.9 ± 3.8	61.9 ± 2.3	63.1 ± 5.7
(2)	80.7 ± 6.6	78.7 ± 2.2	69.1 ± 5.2	58.1 ± 2.9	37.2 ± 2.1	49.0 ± 3.6	52.1 ± 1.0	69.4 ± 4.5
(3)	4.3 ± 0.6	8.1 ± 1.6	4.8 ± 0.4	2.6 ± 0.2	1.9 ± 0.6	1.8 ± 0.3	3.3 ± 0.9	3.6 ± 0.5
(4)	3.2 ± 0.4	6.9 ± 0.8	4.2 ± 0.2	2.4 ± 0.3	1.3 ± 0.2	1.8 ± 0.3	2.2 ± 1.8	3.0 ± 0.3
CIS	11.2 ± 0.5	11.0 ± 0.5	16.5 ± 1.0	19.9 ± 0.9	24.5 ± 2.8	11.4 ± 1.6	21.3 ± 0.1	37.4 ± 6.2
DXR	1.9 ± 0.2	4.6 ± 0.2	2.3 ± 1.8	1.8 ± 0.3	2.5 ± 1.3	3.8 ± 1.6	4.5 ± 0.1	2.5 ± 0.3

Data are presented as the means ± S.E.M. of IC_{50} values in μM obtained by nonlinear regression from at the least three independent experiments performed in triplicate, measured by Alamar blue assay after 24 h incubation. Cancer cells: A549 (human lung carcinoma); Caco-2 (human colorectal adenocarcinoma); DU-145 (human prostate carcinoma); HepG2 (human hepatocellular carcinoma); PC-3 (human prostate adenocarcinoma) and MDA-MB-231 (human breast adenocarcinoma). Non-cancer cells: FGH (human mouth fibroblast) and HUVEC (human umbilical vein endothelial cells). The precursor complexes *bis*-bipyridine (BB), *bis*-phenanthroline (BP), *bis*-diphenylphosphinomethane:bipyridine (DB), diphenylphosphinomethane:phenanthroline (DP) and the ligand lawsone (LAW) were used as controls. Cisplatin (CIS, Fauldcispla®) and doxorubicin (DXR, Fauldoxo®) were used as positive controls.

Table 2
Selectivity index of the Ru complexes.

		Cancer cells					
Non-cancer cells		A549	Caco-2	DU-145	HepG2	PC-3	MDA-MB-231
FGH	(1)	0.7	1.2	1.8	1.4	1.2	1.2
	(2)	1.1	1.4	2.2	1.6	1.5	1.2
	(3)	0.9	1.6	2.3	2.4	1.3	0.8
	(4)	0.8	1.3	2.5	1.8	1.4	1.0
	CIS	0.7	0.6	0.4	1.0	0.5	0.3
	DXR	0.8	1.0	0.7	0.5	0.4	0.7
HUVEC	(1)	0.9	1.5	2.2	1.7	1.5	1.4
	(2)	1.1	1.3	2.1	1.6	1.5	1.1
	(3)	1.6	3.1	4.2	4.5	2.4	2.2
	(4)	1.6	2.8	5.3	3.8	3.1	2.3
	CIS	0.6	0.5	0.4	0.9	0.5	0.2
	DXR	2.0	2.5	1.8	1.2	1.0	1.8

Data are presented with the selectivity index (SI) calculated using the following formula: SI = IC_{50}[non-cancer cells]/IC_{50}[cancer cells]. Cancer cells: A549 (human lung carcinoma); Caco-2 (human colorectal adenocarcinoma); DU-145 (human prostate carcinoma); HepG2 (human hepatocellular carcinoma); PC-3 (human prostate adenocarcinoma) and MDA-MB-231 (human breast adenocarcinoma). Non-cancer cells: FGH (human mouth fibroblast) and HUVEC (human umbilical vein endothelial cells). Cisplatin (CIS – Fauldcispla®) and doxorubicin (DXR – Fauldoxo®) were used as positive controls.

significantly reduce the colony-forming at the same concentrations analyzed ($p > 0.05$).

In complementary to conventional cell monolayer cytotoxic assays performed, we also established 3D multicellular tumor spheroids (MCTS) based on DU-145 cells and used this model for investigating the activity of the ruthenium phosphine complexes toward prostate carcinoma spheroids. The MCTS is a well-established 3D *in vitro* model system that closely reflects the *in vivo* tumor environment concerning nutrient and oxygen gradients, hypoxic/necrotic regions, cell-cell matrix interactions, and gene expression profiles [45]. Therefore, the MCTS was introduced to mimic solid tumors *in vitro* and to study the viability of DU-145 cancer cells treated with the Ru(II) complexes once this model represents a great tool for drug discovery [46,47]. Spheroids grown in ultra-low attachment 96-well plates for 5 days were treated with complexes (**3**) and (**4**) for a period of 24 h to determinate the MCTS viability and were examined for morphological changes until 12 days. The Alamar Blue assay showed that complexes (**3**) and (**4**) reduced the viability of DU-145 MCTS after treatment (Fig. 3A). In general, DU-145 MCTS showed more considerable resistance to both complexes compared to the 2D-cultured cells. Indeed, the MCTS are typically more resistant to antiproliferative compounds because of the differences in the drugs penetration and varying microenvironments (such as pH, hypoxia, extracellular matrix) within spheroids [48]. Similar to *in vivo* tumors, the hypoxic regions inside the spheroids reduces the rate of cell division impairs the effects of anti-proliferative drugs such as cisplatin [49].

Interestingly, the cells in the spheroids showed morphological changes, indicating an effective permeability into spheroid and, therefore, cytotoxicity. The treatment with complex (**4**) disrupted the cell aggregations, resulting in the presence of cell debris after 9 days, suggesting disturbance in cell-matrix interactions (Fig. 3B). The IC_{50} of the complexes (**3**) and (**4**) was 4.1 and 3.4 μM, respectively, while cisplatin presented IC_{50} of 62.6 μM. The complex (**4**) was more potent than cisplatin at the least 18-fold, demonstrating that its cytotoxic activity is effective in the tumor microenvironment, independent of hypoxia. Therefore, (**4**) was selected for detailed studies of the mechanism of cell death.

2.4. The complexes reduce DU-145 cell adhesive and migratory potential

Afterward, cell adhesion and migration assays were performed to evaluate the antimetastatic capability of the complex (**4**). Cancer metastasis mainly occurs due to the migration and adhesion of neoplastic cells from a primary tumor to distant sites following angiogenesis and tumor growth [50]. Therefore, in this research, the anti-migratory and anti-adhesive effects of the complex (**4**) were investigated by wound healing and extracellular matrix adhesion assay on DU-145 cells. For this assays, the cells were treated with concentrations below the IC_{50} values of (**4**) (1.3 ± 0.2 μM, in 24 h). As seen in Fig. 4, untreated DU-145 monolayers were wounded at 0 h and images were registered at different time points after the treatment. The wound space was reduced severely in size in the absence of compounds because of cell proliferation and migration. Complex (**4**) inhibits the cell migration of DU-145 cells, exhibiting deeply reduced wound healing patterns after 48 h were the cells exposed to 0.5 μM presents inhibition of 80% of wound closure, compared to control at the same time. Indeed, the complex (**4**) as expectedly showed an antimetastatic feature, in accordance with the previously reported studies of anti-migratory and anti-angiogenic effects of others ruthenium complexes containing phosphines and diimines as ligands [28,51]. These data demonstrate that low concentrations of (**4**) impaired the androgen-metastatic prostate cancer DU-145 cells migratory potential.

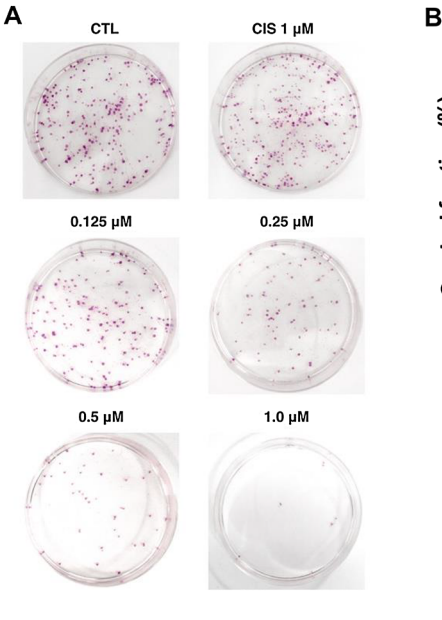

Fig. 2. Assessment of colony survival by clonogenic assay. (A) Representative colony formation images of DU-145 cells after treatment with complex (4). (B) The survival fractions after 24 h treatment with 0.125; 0.25; 0.5 and 1 μM of (3), (4) and cisplatin against DU-145 cells. The negative control (CTL) was treated with the vehicle (0.1% DMSO) used for diluting the tested compound. Data are presented as the means ± S.E.M. of three independent experiments performed in triplicate. $^{*}p < 0.05$ compared with the control by ANOVA followed by Dunnet's test.

Next, we assessed the cell adhesion inhibition of complex (**4**) using mimic extracellular matrix (ECM) adhesion assay. The *in vivo* binding of cells to the extracellular matrix (ECM) is fundamental for cell survival and cell-to-cell communication but is also essential for the metastatic potential of cancer cells [52]. DU-145 cells were incubated to adhere to either collagen or Matrigel® in the presence of different concentrations of the complex (**4**) and assessing the relative numbers of attached cells. As measured by colorimetric assay, untreated and vehicle-treated (CTL) cells exhibited similar adhesion to collagen (Fig. 5A) or Matrigel® (Fig. 5B). The treatments of DU-145 cells with different concentrations of the complex (**4**) significantly inhibited the cell adhesion in a concentration-dependent manner. At 0.5 μM the maximum inhibition of

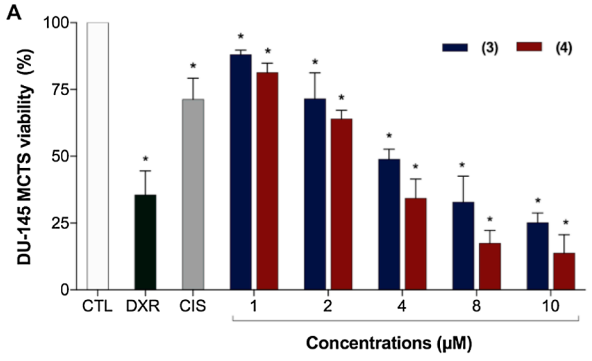

Spheroids	IC_{50} in μM		
	(3)	(4)	CIS
DU-145	4.1 ± 0.1	3.4 ± 0.5	62.6 ± 3.2

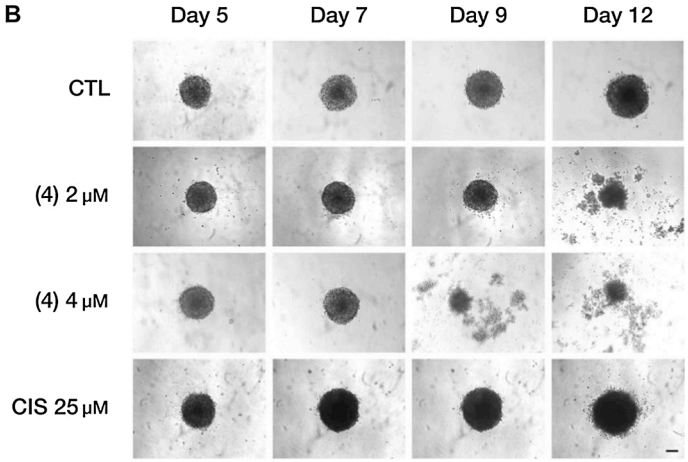

Fig. 3. Effects of the complex (3) and (4) in 3D *in vitro* model of multicellular tumor spheroids of DU-145 cells. (A) The MCTS viability determined by Alamar Blue assay after 24 h treatment and IC_{50} values in μM obtained by nonlinear regression from at the least three independent experiments performed in triplicate. The negative control (CTL) was treated with the vehicle (0.1% DMSO) used for diluting the compounds tested. Doxorubicin (DOX, Fauldoxo® 5 μM), Cisplatin (CIS, Fauldcispla® 25 μM) were used as the positive controls. (B) DU-145 MCTS were examined using inverted microscope (amplification 200×), scale bar = 100 μm. Data are presented as the mean ± S.E.M. of three independent experiments performed in triplicate. $^{*}p < 0.05$ compared with the control by ANOVA followed by Dunnet's test.

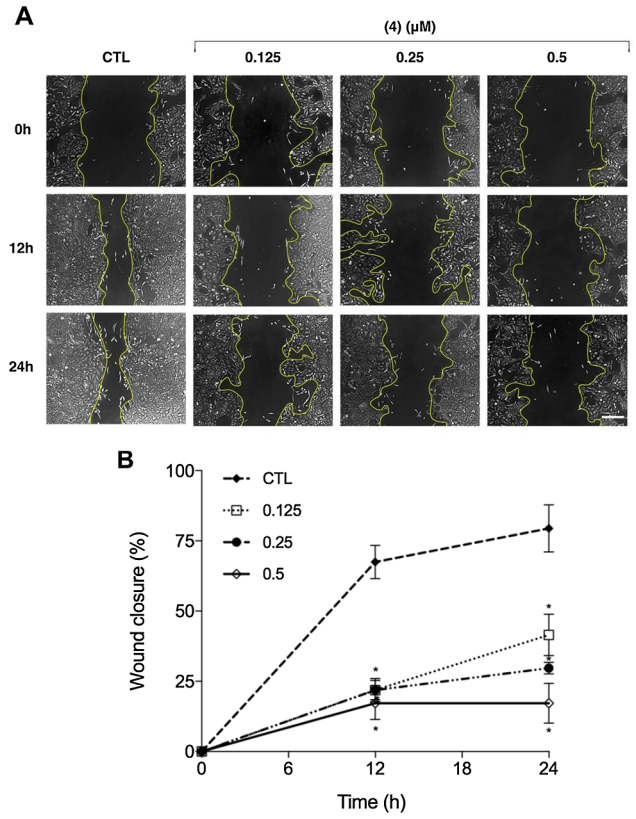

Fig. 4. Inhibitory effects of the complex (4) on DU-145 cells migration *in vitro*. (A) Representative photographs taken at 0, 24 and 48 h post-wound using inverted microscope (amplification 100×), scale bar = 200 μm. The cell monolayer was wounded by a 100 μL pipette tip followed by treatment with different concentrations (0.125, 0.25, and 0.5 μM) of (4) for 24 h. The distance of the wound edge was measured before and after the treatments. (B) Quantification of the relative migration by wound closure. Wound closure (%) were identified from measurements of the migration distance of DU-145 cells from the control group and with complex (4) treatment. Data are presented as the mean ± S.E.M. of three independent experiments performed in triplicate. $^{*}p < 0.05$ compared with the control by ANOVA followed by Dunnet's test.

DU-145 adhesion was calculated by more than 70% on Matrigel® matrix. The anti-metastatic activity of ruthenium compounds is well-recognized by NAMI-A studies [53]. Furthermore, current studies suggest Ru-based complexes inhibits the formation of tube-like structures, an essential step in angiogenesis and metastasis [54]. Our findings indicate that complex (**4**) reduce the ability of DU-145 cells to adhere to ECMs which may impact on their metastatic capacity.

2.5. DNA interactions

The DNA is the most studied targets when it comes to the development of compounds with antitumor properties. It occurs because the interaction between DNA and compounds can cause irreversible damage and prevent cell replication, leading to cell death [55]. In this context, we investigated the ability of the ruthenium complexes to interact with DNA by Circular Dichroism (CD), fluorescence and gel electrophoresis.

The CD technique can be used to analyze the conformation changes in the secondary structure of the calf-thymus DNA (CT-DNA) by monitoring the two bands in the UV region, a positive band at 275 nm and a negative band at 245 nm, due to base stacking and right-handed helicity, respectively. Thus, the CT-DNA was incubated with ruthenium complexes in different molar ratios (0.1–0.4), and the bands were analyzed, and the effects are shown in Fig. 6 for complex (**4**). The intensities of negative and positive bands of the CT-DNA did not show any significant change in intensity upon addition of the ruthenium complex, and the same behavior was observed for all complexes (**1**–**4**).

The ability of the complexes to change the tertiary structure of DNA was investigated by electrophoresis in agarose gel employing the pBR322 plasmid DNA, upon incubation with ruthenium complexes in different molar ratios. Alterations in the electrophoretic mobility of plasmid DNA on agarose gel is commonly considered as evidence for direct DNA–metal interactions. Modification of the DNA structure causes hindrance in the migration of supercoiled DNA and a slight improvement in the mobility of open circular DNA to a feature where both forms comigrate. The pBR322 presents three forms, OC (open circular), L (linear) and CC (supercoiled), which show different electrophoretic mobility. Fig. 7 shows the effect of ruthenium complexes on the mobility of pBR322 after incubation at 37 °C for 18 h. The control in lane 2 refers only to pBR322, and the lines 3–11 correspond to the pBR322 in the presence of complexes (3) and (4). The complexes were capable of affecting the mobility of the bands of pBR322, mainly to OC

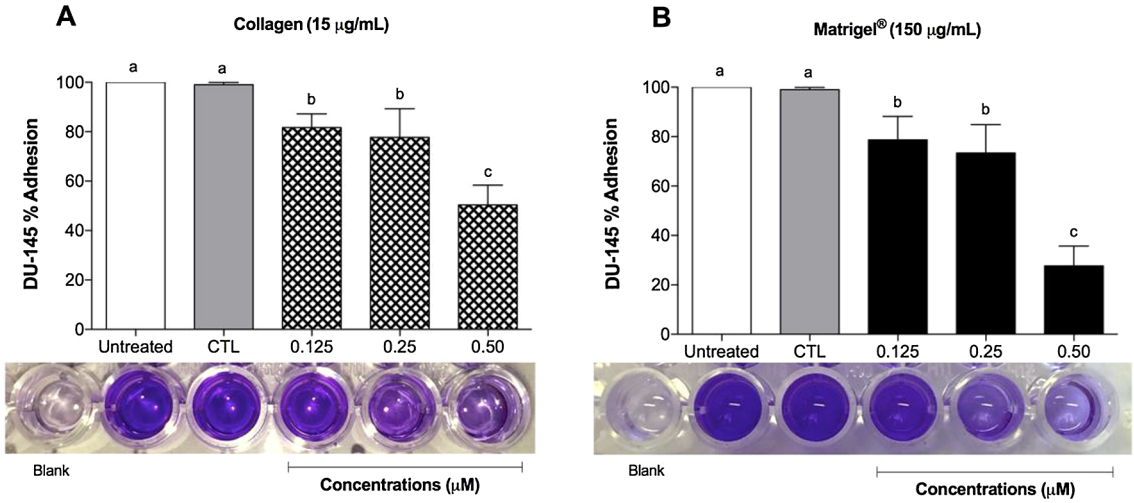

Fig. 5. Complex (4) significantly decreased DU-145 cells adhesive rate on collagen and Matrigel® matrixes. DU-145 cells in the presence of 0.125, 0.25 and 0.5 μM were seeded into 96 well plates coated with collagen (A) and Matrigel® (B) and allowed adhere for 24 h after which supernatants were removed and adhered cells washed and stained with crystal violet. Plates were assayed on a plate reader at 590 nm. Data are presented as the mean ± S.E.M. of three independent experiments performed in triplicate. Values not sharing the same letter are significantly different from each other ($p < 0.05$; ANOVA followed by the Tukey's test).

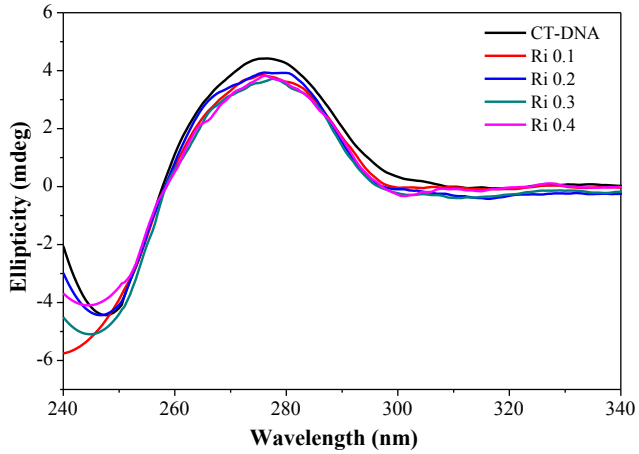

Fig. 6. Fluorescence emission spectra of complex (4) in the presence of increasing amounts of CT-DNA. CD spectra of CT-DNA (50 μM) in the absence and presence of complex (1) in different molar ratio (Ri = [complex (4)]/[DNA], after 18 h of incubation at 37 °C.

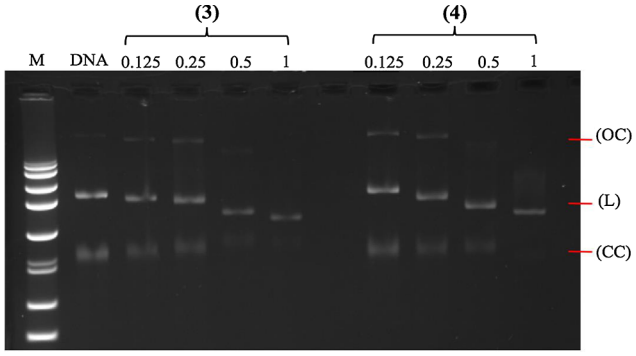

Fig. 7. Electrophoresis mobility of pBR322 plasmid DNA with increasing amounts of complexes (3) and (4) after 18 h of incubation at 37 °C.

and CC bands at Ri 0.5 and 1. The complex (4) was found to exhibit nuclease activity followed by conversion of CC into L, proposing single strand DNA cleavage and the amount of nicked DNA increased at 1 μM showing complete disappearance of CC.

To gain more information about the interaction of complexes with DNA the competition assay using the Hoechst 33258, the fluorescent dye that interacts with DNA through the minor groove, was performed. DNA binding dyes are extensively used to study the mode of drug-DNA interaction. Hoechst 33258 produce a weak fluorescence, but when it binds to DNA a significant increase in fluorescence at 455 nm is observed when excited at 343 nm, thus, it is used as a probe to monitor compounds that interact with DNA [56–58]. Fig. 8 shows the fluorescence spectra of the Hoechst-CT-DNA upon successive addition of complex (**4**). The complex (**4**) was able to decrease the fluorescence of the Hoechst-CT-DNA system with increasing of the concentration, indicating that the complex (**4**) interact with DNA by the minor groove and compete with Hoechst, removing it from DNA structure and consequently, decrease the fluorescence of the system. The same behavior was observed to all ruthenium complexes (Figs. S3–S6 of Supplementary Information). Taken together all the assays employed to investigate the interaction with DNA, we can conclude that ruthenium complexes interact with DNA via the minor groove.

2.6. The complexes induce apoptosis via the BAX/BCL-2 pathway in DU-145 cells

Apoptosis is acknowledged as an essential physiological process in tissue homeostasis. Nevertheless, some cancer cells may adapt to high

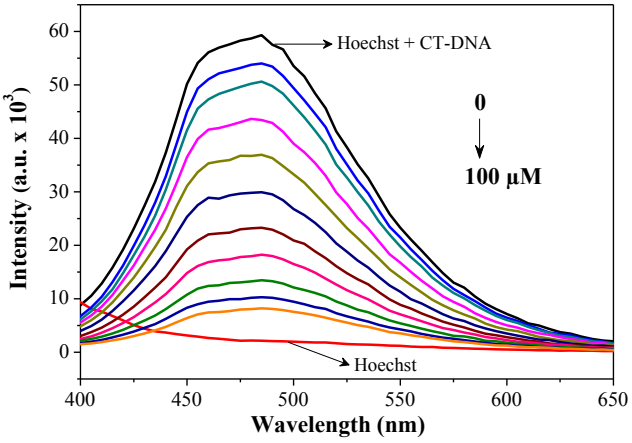

Fig. 8. Emission spectra of Hoechst (2.7 μM, λ_{ex} = 343 nm), CT-DNA (125 μM) in presence of the complex (4) in different concentrations (0–100 μM), at 37 °C.

levels of oncogenic signaling by disabling their senescence- or apoptosis-inducing circuitry. This acquired resistance is appreciated as a hallmark of almost all types of cancer [58,59]. To evaluate whether the complex (**4**) presents the ability to induce apoptosis or necrosis, we selected its concentrations that have shown cytotoxic activity. Therefore, nuclear morphology was assessed by Hoechst 33342/propidium iodide (PI) staining technique for fluorescence microscopy. The results clearly showed that complex (**4**) might induce apoptosis of DU-145 cells based on its staining and morphological characterization after treatments (Fig. 9A).

To determine the percentage of apoptosis and necrosis, the DU-145 cells were treated with 0.25–2.0 μM of the complex (**4**) for 24 h followed by annexin V-FITC/PI staining, and the results were analyzed by using flow cytometry. In live cells, phosphatidylserine (Ptd-L-Ser) is located on the cytoplasmic surface of the cell membrane. The exposure of Ptd-L-Ser on the outer leaflet of the plasma membrane is the final event of apoptosis and can be detected by the binding of fluorescently labeled annexin V [60]. Therefore, annexin V-FITC/PI dual staining can be used to quantify the different cell phenotypes that occur during apoptosis. The percentages of early apoptotic, late apoptotic, necrotic and living cells of DU-145 are shown in Fig. 9B. The incubation of DU-145 cells with increasing concentrations of the complex (**4**) produced a considerable increase in the percentage of apoptotic cells (Q2 and Q4 quadrants) (Fig. 9C). The population of apoptotic cells treated with complex (**4**) had increased remarkably with dose-dependent relation (6.30% for control group, 19.1% for 0.25 μM, 30.9% for 0.50 μM, 45.1% for 1.0 μM and 66.8% for 2.0 μM). Cisplatin treatment at the fixed concentration of 25 μM (IC_{50}) showed 19.5% of apoptotic cells. Therefore, a 100-fold lower concentration of (4) was required for the same effect of cisplatin on DU-145 cells. None of the concentrations induced a significant increase in necrotic cells. Indeed, ruthenium complexes with different ligands have been lead to the apoptosis through the mitochondria, death receptor and oxidative stress pathways [34,61,62]. The molecular mechanism underlying the apoptotic effect of the complex (**4**) was assessed at the level of mRNA expression of pro-apoptotic and anti-apoptotic genes. The 24 h treatment with complex (**4**) at 1.5 μM (IC_{50}) upregulated *BAX* expression by 2.73-fold and downregulated the expression of the gene *BCL-2* by 2.40-fold (Fig. 9D). *BAX* and *BCL-2* are two members of a gene family involved in the regulation of cellular apoptosis. Gene expression analysis revealed that complex (**4**) induced an increase of the expression of the pro-apoptotic *BAX* gene and a decrease of the expression of the anti-apoptotic *BCL-2*. Cells with a high *BAX/BCL-2* ratio will be more sensitive to given apoptotic stimuli when compared to a similar cell type with a comparatively low *BAX/BCL-2* ratio [63]. Therefore, the altered ratio might be an essential key question to understand the sensitizing effect

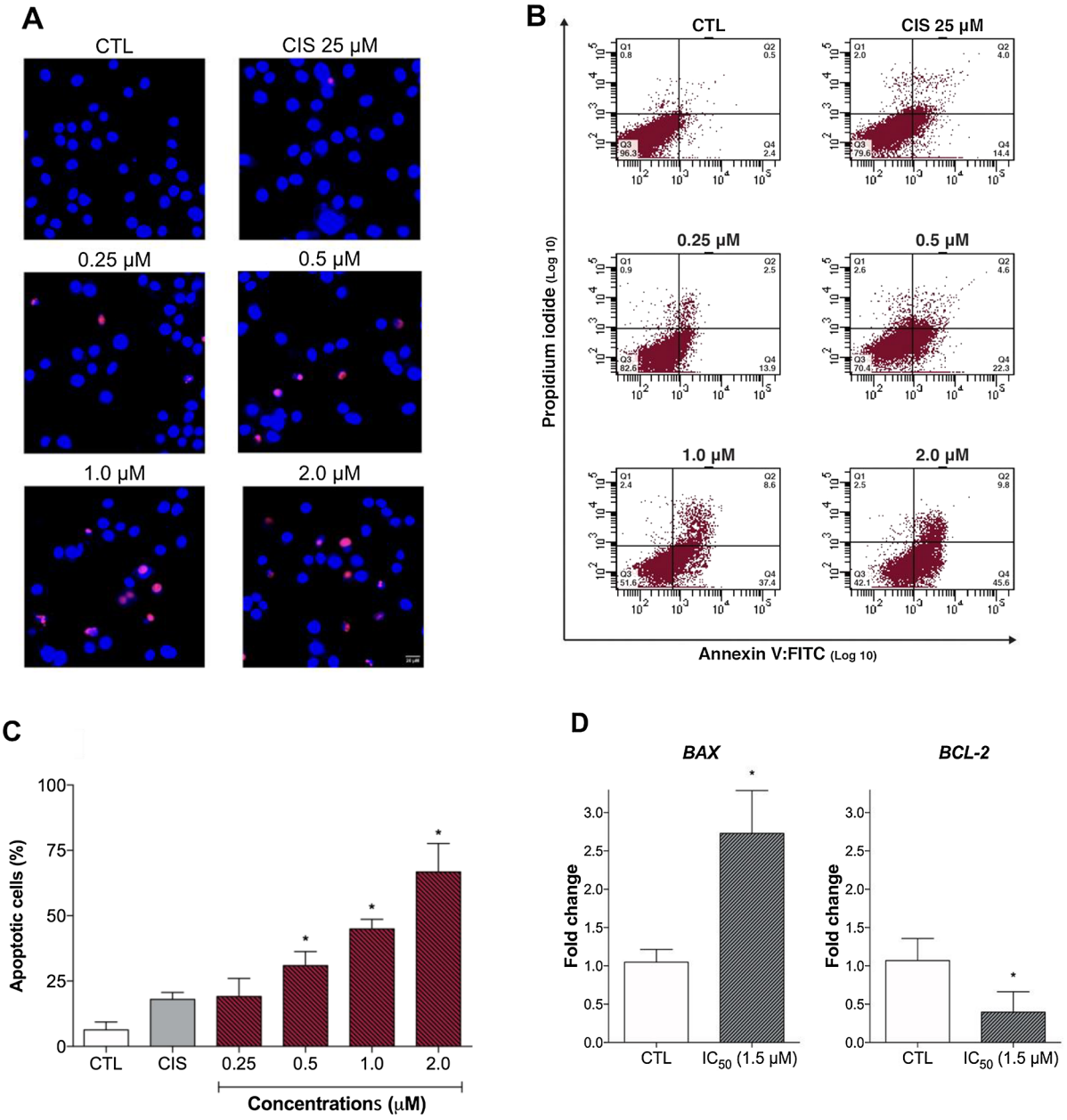

Fig. 9. Effect of the ruthenium complex (4) on the induction of apoptosis in DU-145 cells. (A) Representative images of DU-145 cells double-stained with Hoechst 33342 and PI captured with ImageXpress micro, scale bar = 20 μm. (B) Representative flow cytometry dot plots show the percent cells in the viable (Q3), early apoptotic (Q4), late apoptotic (Q2) and necrotic (Q1) stages as determined by flow cytometry using annexin V-FITC/PI staining. (C) Quantification of apoptotic DU-145 cells. (D) Relative expression of the genes *BAX* and *BCL-2* in DU-145 cells treated with complex (4) for 24 h. *ACTB* was used as reference gene for normalization. The negative control (CTL) was treated with the vehicle (0.1% DMSO) used for diluting the tested compound and cisplatin (CIS, 25 μM) was used as drug control. Data are presented as the means ± S.E.M. of three independent experiments performed in triplicate. Ten thousand events were evaluated per experiment, and cellular debris was omitted from the analysis. *$p < 0.05$ compared with the control by ANOVA followed by Dunnet's test.

of the complex (**4**) in DU-145 cells. Thus, our results demonstrated that complex (**4**) induced cell death by up-regulation of *BAX* and down-regulation of *BCL-2* in DU-145 cancer cells.

2.7. Scavenging intracellular ROS abolishes the cytotoxic effects of the complex (4)

It has been reported that ROS play an important role in cancer cell death and apoptosis. This activity is widely induced by several chemotherapeutic drugs to kill the cancer cells [64]. To investigate whether ROS production is underlying the cytotoxic activities of the complex (**4**), we used the Cellular ROS/Superoxide Detection Assay (ab139476) to detect the production of reactive species of oxygen and nitrogen (ROS/RNS) in DU-145 cells. Previously, the total ROS levels were assessed after a 1, 6, 12 and 24 h of incubation with the complex (**4**) using 2′,7′-dichlorodihydrofluorescein diacetate (H_2DCFDA) as a fluorescent dye to determine which time would be more appropriate for a ROS/Superoxide analysis.

As shown in Fig. 10A, upon treatment of DU-145 cells for different times with a single dose of the complex (**4**) (IC_{50}), a higher increase of ROS generation was observed at 24 h of exposure. Due to this result, the ROS/Superoxide production was assessed after 24 h of treatment with

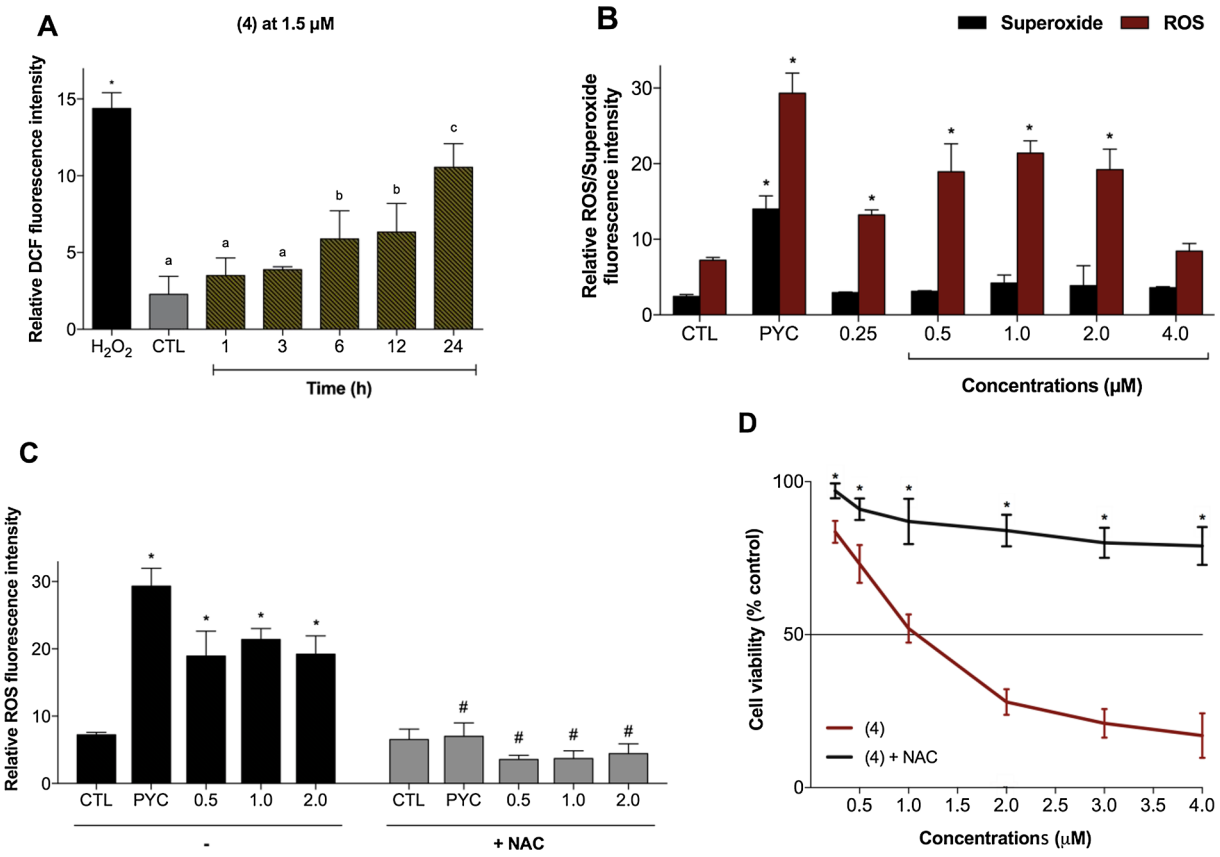

Fig. 10. Effect of the ruthenium complex (4) in the levels of reactive oxygen species (ROS) of DU-145 cells and protection by NAC. (A) ROS levels of DU-145 cells after 1, 3, 6, 12 and 24 h of incubation with complex (4) at IC_{50} (1.5 µM). (B) Assessment of total intracellular ROS/Superoxide levels 24 h after incubation with different concentrations of (4). (C) ROS levels of DU-145 cells after 24 h treatment with complex (4) at 0.5, 1 and 2 µM with or without the antioxidant NAC (5 mM). (D) Cell viability of DU-145 cells assessed by Alamar Blue assay after 24 h incubation with different concentrations of (4) with or without the antioxidant NAC (5 mM). The negative control (CTL) was treated with the vehicle (0.1% DMSO) used for diluting the tested compounds. Hydrogen peroxide (H_2O_2, 200 µM) and pyocyanin (PYC, 250 µM) were used as the positive controls. Data are presented as the mean ± S.E.M. of three independent experiments performed in triplicate or quadruplicate. $^{*}p < 0.05$ compared with the control by ANOVA followed Dunnet's test. # $p < 0.05$ compared with the respective treatment without NAC by ANOVA followed Dunnet's test. Values not sharing the same letter are significantly different from each other ($p < 0.05$; ANOVA followed by the Tukey's test).

different concentrations of the complex (**4**). After the complex (**4**) treatment, DU-145 cells exhibited an increase of reactive species, yielding a fluorescent product indicative of cellular production of different ROS/RNS types (Fig. 10B). Moreover, at 4 µM was observed a decrease of ROS/RNS levels, probably because increasing concentrations promotes cell death. These results indicate that complex (**4**) can enhance intracellular oxidative stress suggesting that apoptosis may be the principal mechanism of cell death triggered by ROS. This effect can be guaranteed by the use of lawsone that has a mechanism of action closely related with their electron accepting capability producing semiquinone radicals that can induce ROS production in the intracellular environment [65]. On the other hand, the production of superoxide did not appear in any treatment of the complex (**4**), except in inducer control (pyocyanin).

Besides, to verify whether or not ROS/RNS generation increase is related to the complex (**4**)-induced cytotoxicity, the cells were treated with the ROS-scavenger *N*-acetyl-L-cysteine (NAC), an antioxidant that has been demonstrated to present cytoprotective effects against ROS-induced cell death [66]. The results displayed that co-treatment with NAC suppressed the generation of intracellular ROS induced by complex (**4**) (Fig. 10C) and prevented the reduction of cell viability, as assessed by Alamar Blue assay (Fig. 10D). These findings suggest that the complex (**4**) played an essential role in inducing apoptosis, just as other naphthoquinones derivatives compounds do [67], by induced increasing oxidative stress, which was prevented by co-treatment with NAC.

3. Conclusions

In this paper, novel lawsone-containing ruthenium(II) complexes were synthesized and assessed for its cellular response in human prostate carcinoma DU-145 cells in 2D and 3D culture systems for the first time. As discussed, other studies have shown that ruthenium complexes have been extensively reported as anticancer candidates *in vitro* and *in vivo* [6,68,69]. Herein we proposed lawsone as a bioactive natural compound that forms ruthenium complexes with potent cytotoxic activity in cancer cells. Overall, the phosphine complexes studied in this work showed promising values of IC_{50} against DU-145 prostate cancer cells. Complexes (**3**) and (**4**) displayed more potent cytotoxicity than metal-free lawsone against different cancer cell lines and can decrease the survival of DU-145 cells at lower concentrations better than cisplatin. Several studies shown the addition of phosphine ligand increase the lipophilicity of the complex, which in turn enhances the cytotoxic effect against several cancer cell lines [70–73]. This effect is related with the enhanced lipophilicity which considerably affecting the uptake by tumor cells and proteins binding [41,74]. Our ruthenium complexes, especially the complex (**4**), exhibited considerable cytotoxic effects against 3D multicellular DU-145 spheroids that simulate the prostate tumor microenvironment. The compound also exhibited cytotoxic potency over 18-fold orders of magnitude higher than cisplatin in monolayers of DU-145 cancer cells and for 3D multicellular DU-145 tumor spheroids. Even under a low non-cytotoxic concentration of 0.125–0.5 µM, (**4**) was able to effectively inhibit the cell adhesion and

migration of DU-145 cells indicating antimetastatic potential *in vitro*. Taken together, all the complexes (**1–4**) showed an effective DNA interactive abilities via DNA minor groove intercalation, which can be considered very valuable taking into account the importance of the history and development of DNA intercalators as anticancer agents. Additionally, complex (**4**) induced DU-145 cell apoptosis through elevated intracellular ROS levels. Moreover, we also showed that ROS scavenger NAC reduced cytotoxicity induced by ROS production caused by the complex (**4**). In summary, this study describes a series of newly synthesized phosphine/diimine ruthenium complexes containing the 1,4-naphthoquinone that have been identified as a potent antiproliferative and antimetastatic agents towards DU-145 cells. By our data, we suggest the coordination with naphthoquinone bioligand enhance ROS-induced apoptotic cell death via upregulation of *BAX/BCL-2* ratio. Therefore, the 1,4-naphthoquinone-containing ruthenium complexes showed a promising anticancer activity better than cisplatin toward prostate cancer cells, target the intracellular oxidative stress.

4. Experimental

4.1. Materials

4.1.1. Chemical and equipments

All chemicals used to prepare the ruthenium complexes were of analytical grade or chemically pure grade. The synthesis of the complexes were carried under argon atmosphere. The $RuCl_3{\cdot}3H_2O$ (CAS 13815-94-6), KPF_6 (CAS 17084-13-8), triphenylphosphine (PPh_3, CAS 603-35-0), *bis*(diphenylphosphino)methane (dppm, CAS 2071-20-7), N-N = 2,2′-bipyridine (bipy, CAS 366-18-7), 1,10-phenanthroline (phen, CAS 66-71-7), resazurin sodium salt (CAS 62758-13-8), calf-thymus DNA (CT-DNA, CAS 73049-39-5), dimethylsulfoxide (DMSO, CAS 67-68-5), dimethylformamide (DMF, CAS 68-12-2), methanol (CAS 67-56-1), acetic acid (CAS 64-19-7), Triton™ X-100 (CAS 9002-93-1), 2′,7′-dichlorofluorescein diacetate (H_2DCFDA; CAS 4091-99-0), hydrogen peroxide solution 30% (w/w) (H_2O_2; CAS 7722-84-1) agarose (CAS 9012-36- 6), collagen (CAS 9007-34-5), trypan blue (CAS 72-57-1), crystal violet (CAS 548-62-9), *N*-acetyl-L-cysteine (NAC, CAS 616-91-1) and pBR322 plasmid DNA from *E. coli* (CAS 93384-17-9) were obtained from Sigma-Aldrich® MERCK (St. Louis, MO, USA). Fetal bovine serum (FBS), Dulbecco's Modified Eagle's Medium (DMEM), Roswell Park Memorial Institute Medium (RPMI 1640), trypsin-EDTA 5X, accutase, L-glutamine, antibiotic-antimycotic mix 100X, Hoechst 33342 (CAS 23491-52-3) and propidium iodide (PI; CAS 25535-16-4) were acquired from Gibco-Invitrogen® Thermo Fisher Scientific (Waltham, MA, USA). Matrigel® matrix was obtained from Corning (New York, NY, USA). Fauldcispla® (cisplatin) and Fauldoxo® (doxorubicin hydrochloride) were purchased from Libbs Pharmaceutical Ltda. (São Paulo, SP, Brazil). All the other chemicals were of analytical grade.

Elemental analyses (C, H, and N) were performed using a FISIONS CHNS, model EA 1108 Thermo Fisher Scientific (Waltham, MA, USA) equipment. The IR spectra were recorded on an FT-IR Bomem-Michelson 102 spectrometer in the 4000–250 cm^{-1} region using KBr pellets. Conductivity measures were obtained in a Meter Lab CDM2300 using 10^{-3} M solutions of the complexes in CH_2Cl_2, at room temperature. All the NMR experiments were recorded on a Bruker DRX 400 MHz using tetramethylsilane as reference and DMSO-d_6 to solubilize the complexes. UV–visible (UV–vis) was recorded on a Hewlett Packard diode array − 8452A spectrophotometer. Fluorescence spectra were performed using a Synergy H1 Fluorescence Spectrophotometer (BioTek®). The electrochemical experiments were carried using a BAS, model 100B at room temperature in CH_2Cl_2 containing 0.10 M tetrabutylammonium perchlorate (TBAP) (Fluka Purum®) as a supporting electrolyte. The working and auxiliary electrodes were stationary Pt foils, and the reference electrode was Ag/AgCl, 0.10 M TBAP in CH_2Cl_2, in a Luggin capillary probe.

4.1.2. Cell lines and culture conditions

Human lung carcinoma (A549, ATCC® CCL-185™), human prostate carcinoma (DU-145, ATCC® HTB-81™), human hepatocellular carcinoma (HepG2, ATCC® HB-8065™), human prostate adenocarcinoma (PC-3, ATCC® CRL-1435™), human breast adenocarcinoma (MDA-MB-231, ATCC® HTB-26™) and human umbilical vein endothelial cells (HUVEC, ATCC® CRL-1730™) were obtained from American Type Cell Collection (ATCC). Human colorectal adenocarcinoma (Caco-2, BCRJ 0059) and human gingival normal fibroblasts (FGH BCRJ 0089) were obtained from Rio de Janeiro Cells Bank (BCRJ). The cells A549, Caco-2, DU-145, HepG2, MDA-MB-231, and FGH, were cultured in Dulbecco's Modified Eagle's Medium (DMEM), PC-3 and HUVEC cells were grown in Roswell Park Memorial Institute Medium (RPMI 1640). Both mediums were supplemented according to the needs of each lineage, as recommended by its cell banks with 2 mM L-glutamine, 10% or 20% FBS, 1% antibiotic–antimycotic solution (5 mg/mL penicillin, 5 mg/mL streptomycin, and 10 mg/mL neomycin), 4.5 g/L of glucose and 3.7 g/L of $NaHCO_3$. All cell lines were cultured in flasks at 37 °C in 5% CO_2 and 96% of relative humidity according to the procedures proposed by [75]. The experiments were conducted between the third and the eight-cell passage with sub-cultures every 3–4 days to maintain exponential growth. The cell viability was examined using the trypan blue exclusion assay for all experiments where over 90% of the cells were viable at the beginning of the culture.

4.2. Methods

4.2.1. Synthesis and characterization of the ruthenium complexes

4.2.1.1. [Ru(law)(N-N)$_2$]PF$_6$. The complexes [Ru(law)(N-N)$_2$]PF_6 where N-N = bipy or phen were obtained from the reaction between the complex precursor *cis*-[$RuCl_2$(N-N)$_2$] prepared how described by [76] and the ligand lawsone (law). The ligand law (0.054 g; 0.31 mmol) was added to the solution of ethanol and water (2:1 v/v) (30 mL) with the complex precursor (0.21 mmol), 80 μL of triethylamine and KPF_6 (0.076 g; 0.41 mmol). The mixture was maintained in argon atmosphere and reflux for 12 h. The dark solution was concentrated to ca. 5 mL and the solid formed was filtered, washed with distilled water and ethyl ether and dried under vacuum.

[Ru(law)(bipy)$_2$]PF_6 (**1**): Yield: 0.113 g (75%). Anal. Calc. For $C_{30}H_{21}F_6N_4O_3PRu$ exp. (calc.) C, 49.03 (49.25); H, 3.29 (2.89); N, 7.73 (7.66) %. Λ_M = 49.81 Ω^{-1} cm^2 mol^{-1}, in 1.0 mM CH_2Cl_2 solution. IR (Selected bands, cm^{-1}): ν(C_1=O) 1590, ν(C_4=O) 1609, ν(C_2–O) 1027; ^{1}H NMR (400 MHz, DMSO-d_6, 25 °C): δ(ppm): 10.3–7.3 (m, 20H, an overlap of aromatic protons of bipy (16H) and Law (4H), 5.7 (s, 1H, Law); ^{13}C NMR (400 MHz, DMSO-d_6, 25 °C): δ(ppm) 196.9 (C_1=O), 182.7 (C_4=O) and 172.7 (C_2–O).

[Ru(law)(phen)$_2$]PF_6 (**2**): Yield: 0.102 g (70%). Anal. Calc. For $C_{34}H_{21}F_6N_4O_3PRu$ exp. (calc.) C, 52.09 (52.38); H, 2.81 (2.72); N, 6.93 (7.19) %. Λ_M = 44.74 Ω^{-1} cm^2 mol^{-1}, in 1.0 mM CH_2Cl_2 solution. IR (Selected bands, cm^{-1}): ν(C_1=O) 1593, ν(C_4=O) 1612, ν(C_2–O) 1098; ^{1}H NMR (400 MHz, DMSO-d_6, 25 °C): δ(ppm): 10.8–7.4 (m, 20H, an overlap of aromatic protons of phen (16H) and Law (4H), 5.6 (s, 1H, Law); ^{13}C NMR (400 MHz, DMSO-d_6, 25 °C): δ(ppm) 197.3 (C_1=O), 182.5 (C_4=O) and 172.9 (C_2–O).

4.2.1.2. [Ru(law)(dppm)(N-N)]PF$_6$. Firstly, the precursor complexes *cis*-[$RuCl_2$(dppm)(bipy)] and *cis*-[$RuCl_2$(dppm)(phen)] were obtained from the reaction of the *cis,trans*-[$RuCl_2(PPh_3)_2$(N-N)], where N-N = bipy or phen [77] (0.12 mmol) with the dppm (0.14 mmol) in 50 mL of toluene. The reaction was kept in reflux under argon atmosphere for 48 h. The red solid formed was filtered, washed with ethyl ether and dried under vacuum.

The complexes [Ru(law)(dppm)(N-N)]PF_6, where N-N = bipy or phen were obtained from the precursor *cis*-[$RuCl_2$(dppm)(N-N)]. For this, the ligand law (0.04 g; 0.22 mol) was added to the solution of *cis*-[$RuCl_2$(dppm)(N-N)] (0.14 mmol) in 30 mL of CH_2Cl_2:CH_3OH (1:1, v/

v). 80 μL of triethylamine and KPF_6 (0.28 mmol) were added and the reaction kept in reflux under argon atmosphere for 12 h. The volume was reduced to ca. 5 mL and water was added to precipitate a dark solid.

[Ru(law)(dppm)(bipy)]PF_6 (**3**): Yield: 0.129 g (82%). Anal. Calc. for $C_{45}H_{35}F_6N_2O_3P_3Ru$ exp. (calc.) C, 56.26 (56.31); H 3.85 (3.68); N 2.65 (2.92) %. Λ_M = 48.0 Ω^{-1} cm^2 mol^{-1}, in 1.0 mM CH_2Cl_2 solution. IR (Selected bands, cm^{-1}): $\nu(C_1{=}O)$ 1603, $\nu(C_4{=}O)$ 1614, $\nu(C_2{-}O)$ 1097. $^{31}P\{^1H\}$ NMR (162 MHz, CH_2Cl_2, 25 °C) δ(ppm): (d, 17.9; 6.7/15.2; 5.75/^2J = 73/68 Hz); ^1H NMR (400 MHz, DMSO-d_6, 25 °C): δ(ppm): 8.8–6.7 (m, 32H, an overlap of aromatic protons of phenyl groups of dppm (20H), bipy (8H) and Law (4H), 5.8 (s, 1H, Law), 5.4 (m, 2H, chain aliphatic of dppm); ^{13}C NMR (400 MHz, DMSO-d_6, 25 °C): δ(ppm) 200.2/196.8 ($C_1{=}O$), 182.4/181.9 ($C_4{=}O$) and 172.4/171.2 ($C_2{-}O$).

[Ru(law)(dppm)(phen)]PF_6 (**4**): Yield: 0.104 g (78%). Anal. Calc. for $C_{47}H_{35}F_6N_2O_3P_3Ru$ exp. (calc.) C, 57.67 (57.38); H, 3.71 (3.59); N, 2.48 (2.85) %. Λ_M = 50.3 Ω^{-1} cm^2 mol^{-1}, in 1.0 mM CH_2Cl_2 solution. IR (Selected bands, cm^{-1}): $\nu(C_1{=}O)$ 1599, $\nu(C_4{=}O)$ 1614, $\nu(C_2{-}O)$ 1101. $^{31}P\{^1H\}$ NMR (162 MHz, CH_2Cl_2, 25 °C) δ(ppm): (d, 18.2; 6.6/15.4; 6.2/^2J = 74/68 Hz); ^1H NMR (400 MHz, DMSO-d_6, 25 °C): δ(ppm): 9.2–6.3 (m, 32H, an overlap of aromatic protons of phenyl groups of dppm (20H), phen (8H) and Law (4H), 5.8 (s, 1H, Law), 5.5 (m, 2H, chain aliphatic of dppm); ^{13}C NMR (400 MHz, DMSO-d_6, 25 °C): δ(ppm) 200.3/196.8 ($C_1{=}O$), 182.5/181.9 ($C_4{=}O$) and 172.6/171.4 ($C_2{-}O$).

4.2.2. Partition coefficient (n-octanol/water) determination

The octanol-water partition coefficient (log *P*) were determined using the shake-flask method [78]. Each complex was tested in a mixture of equal volumes of water and *n*-octanol with continuous shaking for 24 h at 112*g* and 37 °C. Then the samples were centrifuged for 5 min at 10*g*, and the organic and aqueous phases were separated. The concentration of drug in each phase was measured spectrophotometrically to determine values of log *P* = [compound] (in *n*-octanol)/[compound] (in water). The experiments were carried out in triplicate.

4.2.3. Cytotoxicity activity assay

The *in vitro* antiproliferative activity was quantified using the Alamar Blue assay, according to the method reported by [79]. Cells were inserted in 96-well plates for all experiments (1.5 × 10^4 cells/well). After 24 h, the complexes were dissolved in DMSO and added to each well and incubated for 24 h. Dilutions of the complexes were prepared to obtain concentrations ranging from 0.3 to 100 μM. Cisplatin (Fauldcispla®) and doxorubicin hydrochloride (Fauldoxo®) were used as the reference cytotoxic drugs. DMSO (0.1% (v/v)) was used as the vehicle control. Following 24 h of incubation, 50 μL of Alamar Blue (resazurin at 0.01% w/v) was added to each well, and the plates were incubated for 2 h, at 37 °C, in the dark. The fluorescence reading was performed in a CaryEclipse Fluorescence Spectrophotometer (Agilent Technologies, Santa Clara, CA, USA) reader using excitation and emission filters at wavelengths of 560 and 590 nm, respectively. The potency of cell growth inhibition for each complex was expressed as half-maximal (50%) inhibitory concentration (IC_{50}).

4.2.4. Clonogenic assay

The clonogenic assay was performed in accordance by the guidelines of [43]. The DU-145 cells (1 × 10^6 cells/well) were inserted in 6-well plate and treated with different concentrations varying of 0.125 to 1 μM of the complexes and cisplatin for 24 h. Negative control received the vehicle (DMSO 0.1% (v/v)) that was used for diluting the compounds tested. At the end of the treatments, the cells were washed with PBS and harvested by trypsinization. The cells were counted using a Neubauer chamber and re-plated then on Nunclon® cell culture dishes of 21.5 cm^2 in a density of two hundred cells per culture dish for each treatment in triplicate. After 7 days cells were washed with PBS and fixed in ice-cold methanol: acetic acid: distilled water (1:1:8) for 20 min, air-dried and stained with crystal violet (0.5% (w/v)) in PBS for 20 min. Colonies with at least 50 cells were counted. The plating efficiency (PE) of DU-145 cells was calculated by the ratio of the number of colonies observed after 7 days of incubation to the number of cells seeded (two hundred). The average of colonies in control was regarded as 100% and the number of colonies that arise after treatment of cells, expressed regarding PE, is called the surviving fraction (SF), obtained by:

$$SF = \frac{Number\ of\ colonies\ counted\ in\ eacht\ treatment}{Number\ of\ colonies\ counted\ in\ control\ x\ PE} \times 100$$

4.2.5. 3D multicellular tumor spheroids culture

The multicellular tumor spheroids (MCTS) were obtained according to the method reported by [80]. Briefly, 200 μL of a solution of DU-145 cells (2.0 × 10^3 cells/well) were inserted in agarose-coated 96-well plates (1.5% (w/v)) and cultured in complete medium plus 3% Matrigel®. DU-145-MCTS with stable structures had formed after five days. Then, the spheroids were exposed to the complexes in a range of five different concentrations varying from 1 to 10 μM and incubated for 24 h. Cisplatin (Fauldcispla®) at 25 μM was used as the reference cytotoxic drug. Negative control received the vehicle (DMSO 0.1% v/v) that was used for diluting the compounds tested. At the end of the experiment, the cell viability was determined by Alamar Blue assay as described above. To investigate the morphological changes after treatment, other MCTSs were examined for 12 days by light microscopy (Inverted Trinocular Microscope Opton TNB-O5T-PL) using AxioVision LE software (Carl Zeiss, Jena, Germany).

4.2.6. Wound healing migration assay

DU-145 cells were seeded at a density of 1 × 10^5 cells per well in 12-well plates and grown for 48 h in 5% CO_2 in a humidified atmosphere at 37 °C in serum-free media. Once confluent, a "wound" was created across the cell monolayer using a sterile pipette. The culture medium containing cells in suspension was removed and replaced with new media containing different concentrations of the complex (**4**). Negative control received the vehicle (DMSO 0.1% (v/v)) that was used for diluting the compounds tested. Images of each wound were recorded using an inverted trinocular microscope (Opton TNB-O5T-PL) coupled to a camera (AxioVision) with amplification of 10×, at different times (0–24 h). The wound closure was analyzed by the recorded images using Image J software.

4.2.7. Cell adhesion

DU-145 cells were seeded at a density of 1.5 × 10^4 cells per well in the presence or absence of different concentrations of the complex (**4**) in pre-coated 96-well plates with either 15 μg/mL collagen or Matrigel® 150 μg/mL and left for 24 h at 5% CO_2 in a humidified atmosphere to adhere. Negative control received the vehicle (DMSO 0.1% (v/v)) that was used for diluting the compounds tested and, cell-free coated wells acted as blank controls. Following adhesion, cells were washed 3x with PBS and fixed with 100 μL methanol at −20 °C for 5 min. Once removed, cells were stained for 15 min with crystal violet (0.1% (w/v)) after which they were rinsed with tap water. Following 10 min air-drying, 50 μL of 0.5% Triton™ X-100 was added to wells and left 2 h at room temperature with gentle agitation. Finally, the absorbance was measured in a spectrophotometer (Biotek Elx800–Winooski, VT, USA) set at 590 nm.

4.2.8. DNA interactions assays

The CT-DNA solution was prepared by dilution of 2 mg of the CT-DNA in 1 mL of Tris-HCl buffer (4.5 mM Tris-HCl, 0.5 mM Tris-base, 50 mM NaCl, pH 7.4), and the concentration was determined by absorption spectrophotometric using the molar absorption coefficient 6600 mol^{-1} dm^3 cm^{-1} at 260 nm [81].

4.2.8.1. Interaction with CT-DNA (Calf Thymus) by circular dichroism (CD). The interaction of the ruthenium complexes (**1**–**4**) with CT-DNA by CD was investigated using a spectropolarimeter JASCO J720 from 240 to 350 nm at 298 K, in a continuous scanning mode (200 nm min^{-1}), under constant nitrogen flush. The complexes were incubated with CT-DNA (50 μM) at 37 °C for 18 h in Tris-HCl buffer containing 10% of DMSO for solubilization of the complexes, in molar ratios ([complex]/[DNA]) ranging from 0.1 to 0.5.

4.2.8.2. pBR322 plasmid. Plasmid pBR322 (38 μM) was mixed with different concentrations (4.84–38 μM) of ruthenium complexes and incubated at 37 °C for 18 h. Then the loading buffer was added and the samples and analyzed by agarose gel electrophoresis for 90 min in 1% agarose gel using a Tris-acetate-EDTA (TAE) buffer (0.45 M Tris-HCl, 0.45 M acetic acid, 10 mM EDTA, pH 7.4) and employing ethidium bromide for staining. The bands were visualized with a ChemiDoc MP imager (BioRad Laboratories, Hercules, CA, USA).

4.2.8.3. Competitive displacement with Hoechst 33258 by fluorescence. The competitive displacement assay was carried out using as probe the Hoechst 33258 by the fluorescence quenching experiment [57]. Thus, the CT-DNA (125 μM) was incubated with Hoechst (2.7 μM), and the extinction of the fluorescence intensity was monitored by the addition of different concentrations of ruthenium complexes in Tris-HCl containing 10% of DMSO. The fluorescence emission spectra were recorded from 300 to 500 nm after excitation wavelength of 343 nm, using an opaque 96-well plate, in a Synergy/H1-Biotek fluorimeter, at 37 °C.

4.2.9. Apoptosis analyses

The measurement of cell death was performed by the guidelines of [82]. Previously, the nuclear morphology of DU-145 cells was assessed by Hoechst-propidium iodide (PI) dual-staining assay. Briefly, the cells were seeded (5×10^3 cells/well) into black 96-well plates and maintained to attach at 37 °C in 5% CO_2. After 24 h, the cells were treated with complex (**4**) (0.25, 0.50, 1.0 and 2.0 μM) for 24 h. Negative control received the vehicle (DMSO 0.1% (v/v)) and, positive controls received cisplatin (25 μM) and doxorubicin (5 μM). The cells were incubated with Hoechst 33342 (10 μM) and PI (10 μM) diluted in PBS for 10 min at room temperature. The cells were then observed by ImageXpress Micro XLS system (Molecular Devices, CA, USA). The detection of apoptotic/necrotic cells was determined by flow cytometry using the Alexa Fluor® 488 Annexin V/PI (Molecular Probes™) and the analysis were performed according to the manufacturer's instructions. Briefly, DU-145 cells were seeded (5.5×10^4 cells/well) in 12-well plates and maintained to attach at 37 °C in 5% CO_2. After 24 h, the cells were treated as described above. Then, the cells were collected with accutase, washed with PBS and resuspended in 200 μL of cold annexin-binding buffer. Next, it was added 10 μL of Alexa Fluor® 488 Annexin V (50 μL/mL) staining buffer, and the mixture was incubated in the dark at 4 °C for 15 min. Previously the analyses, 100 μL of PI (2 μg/mL) was added, and then, the fluorescence was measured by flow cytometry in a FACSCanto flow cytometer (Becton Dickison, Franklin Lakes, NJ, USA) using the Diva software. Ten thousand events were evaluated per experiment, and cellular debris was omitted from the analysis.

4.2.10. Gene expression analysis by qPCR array

DU-145 cells were plated in bottles tissue culture ($1x10^5$ cells/mL). After 24 h of incubation with complex (**4**) at IC_{50}, total RNA was isolated from the cells using the RNeasy Plus mini kit (Qiagen, Hilden, Germany) according to the manufacturer's instructions. Total RNA was quantified using a spectrophotometer at an absorbance of 260 nm in NanoDrop ND-2000 (Thermo-Fisher Scientific, USA) and the quality of each RNA sample was verified by gel electrophoresis in a Bioanalyzer (Agilent Inc). RNA purity was calculated from the ratio of absorbance $A_{260/280}$ and the integrity by RIN (RNA Integrity Number). Complementary DNA (cDNA) strands were synthesized using the RT^2 First Strand kit (Qiagen, Germany), following the manufacturer's instructions. Quantitative PCR was carried out with the Power SYBR® Green Master Mix in a Step One Plus system (Applied Biosystems, Carlsbad, CA, USA), using KiCqStart® SYBR® Green Primers predesigned for gene expression for mRNA analysis (Sigma-Aldrich), as follows: H_ACTB_1 (NM_001101), H_BAX_1 (NM_004324) and H_BCL2_1 (NM_000633). Quantification of relative fold change of each gene was calculated by $2^{\Delta\Delta Ct}$ method [83] using the reference gene *ACTB* (actin beta) for normalization. All experiments were performed in triplicate in DNase/RNase free conditions.

4.2.11. Detection of intracellular ROS and RNS

The total intracellular ROS generation was measured using H2DCFDA, as reported by [84]. Briefly, DU-145 cells were seeded (1.5×10^4 cells/well) into black 96-well plates and maintained to attach at 37 °C in 5% CO_2. After 24 h, the cells were treated with 1.5 μM (IC_{50}) of the complex (**4**) for 1, 6, 12 and 24 h. After that, the cells were labeled with H2DCFDA solution at 5 μM in DMF. After that, the fluorescence intensity was measured in a Synergy H1 Fluorescence Spectrophotometer (BioTek®), at the excitation and emission wavelengths of 495 and 527 nm, respectively. After that, the ROS/RNS levels were measured using Cellular ROS/Superoxide Detection Assay Kit (Abcam). The cells were seeded (1.5×10^4 cells/well) into black 96-well plates and maintained to attach at 37 °C in 5% CO_2. After 24 h, the cells were treated with complex (**4**) (0.25, 0.50, 1.0 and 2.0 μM) for 24 h. Negative control received the vehicle (DMSO 0.1% v/v), and positive control received pyocyanin (250 μM) as ROS inducer. Following this, the cells were labeled with Oxidative Stress Detection Reagent (Green) for ROS detection and Superoxide Detection Reagent (Orange) according to the manufacturer's instruction. Fluorescence was then measured in quadruplicates using a fluorescent microplate reader Synergy H1 (BioTek®) with standard fluorescein (Ex = 488 nm, Em = 520 nm) and rhodamine (Ex = 550 nm, Em = 610 nm) filter sets for ROS and superoxide determination, respectively.

The protection assays using the antioxidant NAC were also performed. In brief, the cells were treated with 5 mM NAC in association with complex (**4**) (0.25, 0.50, 1.0 and 2.0 μM) for 24 h. The cells were then labeled with H2DCFDA solution, and the ROS levels were measured as described above. In a new set of experiments, the cells were treated with 5 mM NAC in association with cytotoxic concentrations of (**4**). After 24 h of treatment, the cell viability was determined by Alamar Blue assay as described above.

4.3. Statistical analysis

Data are presented as mean ± S.E.M. or as IC_{50} values with 95% confidence intervals (CI 95%) obtained by nonlinear regression. Differences between experimental groups were compared using analysis of variance (ANOVA) followed by the Dunnet's or Tukey's test ($p < 0.05$). All statistical analyses were performed using GraphPad Prism 7 for Mac OS X (Intuitive Software for Science, San Diego, CA, USA).

Acknowledgments

The authors gratefully acknowledge the financial support from the São Paulo Research Foundation (FAPESP, Grants 2016/22429-7, 2016/16312-0 and 2018/00163-0), Coordinating Committee for Advancement of Higher Education Staff in Brazil (CAPES) and National Council for Scientific and Technological Development (CNPq). The authors also thank Mrs. Joana D'Arc Castania Darin from the Department of Clinical Analysis, Toxicology and Food Sciences at FCFRP-USP for her technical assistance.

Appendix A. Supplementary material

Supplementary data to this article can be found online at https://doi.org/10.1016/j.bioorg.2019.02.010.

References

[1] M. Frezza, S. Hindo, D. Chen, A. Davenport, S. Schmitt, D. Tomco, et al., Novel metals and metal complexes as platforms for cancer therapy, Curr. Pharm. Des. 16 (2010) 1813–1825, https://doi.org/10.2174/138161210791209009.

[2] A.M. Florea, D. Büsselberg, Cisplatin as an anti-tumor drug: cellular mechanisms of activity, drug resistance and induced side effects, Cancers (Basel) 3 (2011) 1351–1371, https://doi.org/10.3390/cancers3011351.

[3] G. Sava, S. Pacor, G. Mestroni, E. Alessio, Na[*trans*-RuCl$_4$(DMSO)Im], a metal complex of ruthenium with antimetastatic properties, Clin. Exp. Metastasis. 10 (1992) 273–280, https://doi.org/10.1007/BF00133563.

[4] C.S. Allardyce, P.J. Dyson, Metal-based drugs that break the rules, Dalt. Trans. 45 (2016) 3201–3209, https://doi.org/10.1039/C5DT03919C.

[5] J.K. Barton, E.D. Olmon, P.A. Sontz, Metal complexes for DNA-mediated charge transport, Coord. Chem. Rev. 255 (2011) 619–634.

[6] M. Pal, U. Nandi, D. Mukherjee, Detailed account on activation mechanisms of ruthenium coordination complexes and their role as antineoplastic agents, Eur. J. Med. Chem. 150 (2018) 419–445, https://doi.org/10.1016/j.ejmech.2018.03.015.

[7] S. Zorzet, A. Bergamo, M. Cocchietto, A. Sorc, B. Gava, E. Alessio, et al., Lack of *In vitro* cytotoxicity, associated to increased G(2)-M cell fraction and inhibition of matrigel invasion, may predict *In vivo*-selective antimetastasis activity of ruthenium complexes, J. Pharmacol. Exp. Ther. 295 (2000) 927–933.

[8] C.S. Allardyce, P.J. Dyson, Ruthenium in medicine: Current clinical uses and future prospects, Platin. Met. Rev. 45 (2001) 62–69.

[9] F. Lentz, A. Drescher, A. Lindauer, M. Henke, R.A. Hilger, C.G. Hartinger, et al., Pharmacokinetics of a novel anticancer ruthenium complex (KP1019, FFC14A) in a phase I dose-escalation study, Anticancer. Drugs 20 (2009) 97–103, https://doi.org/10.1097/CAD.0b013e328322fbc5.

[10] S. Leijen, S.A. Burgers, P. Baas, D. Pluim, M. Tibben, E. Van Werkhoven, et al., Phase I/II study with ruthenium compound NAMI-A and gemcitabine in patients with non-small cell lung cancer after first line therapy, Invest. New Drugs. 33 (2015) 201–214, https://doi.org/10.1007/s10637-014-0179-1.

[11] C.O. D'Sousa, J.H. Araujo, I.R.S. Baliza, R.B. Dias, F. Valverde, M.T.A. Vidal, et al., Novel piplartine-containing ruthenium complexes: synthesis, cell growth inhibition, apoptosis induction and ROS production on HCT116 cells, Oncotarget 8 (2017) 104367–104392, https://doi.org/10.18632/oncotarget.22248.

[12] H. Chen, J.A. Parkinson, S. Parsons, R.A. Coxall, R.O. Gould, P.J. Sadler, Organometallic ruthenium(II) diamine anticancer complexes: Arene-nucleobase stacking and stereospecific hydrogen-bonding in guanine adducts, J. Am. Chem. Soc. 124 (2002) 3064–3082, https://doi.org/10.1021/ja017482e.

[13] R.A. De Grandis, F.A. Resende, M.M. Da Silva, F.R. Pavan, A.A. Batista, E.A. Varanda, *In vitro* evaluation of cyto-genotoxic potential of ruthenium(II) SCAR complexes: a promissing class of antituberculosis agents, Mutat. Res. Genet. Toxicol. Environ. Mutagen. 798 (2016) 11–18, https://doi.org/10.1016/j.actamat.2015.02.029.

[14] C. Tan, S. Hu, J. Liu, L. Ji, Synthesis, characterization, antiproliferative and anti-metastatic properties of two ruthenium-DMSO complexes containing 2,2′-biimidazole, Eur. J. Med. Chem. 46 (2011) 1555–1563, https://doi.org/10.1016/j.ejmech.2011.01.074.

[15] V.R. Silva, R.S. Corrêa, L.D.S. Santos, M.B.P. Soares, A.A. Batista, D.P. Bezerra, A ruthenium-based 5-fluorouracil complex with enhanced cytotoxicity and apoptosis induction action in HCT116 cells, Sci. Rep. 8 (2018) 1–13, https://doi.org/10.1038/s41598-017-18639-6.

[16] C. Avendaño, J.C. Menéndez, Medicinal Chemistry of Anticancer Drugs, Elsevier Science, 2008. http://doi.org/10.1016/B978-0-444-52824-7.00001-9.

[17] A.K. McClendon, N. Osheroff, DNA topoisomerase II, genotoxicity, and cancer, Mutat. Res. Fundam. Mol. Mech. Mutagen. 623 (2007) 83–97, https://doi.org/10.1016/j.mrfmmm.2007.06.009.

[18] J.S. Novais, C.S. Moreira, A.C.J.A. Silva, R.S. Loureiro, A.M. Sá Figueiredo, V.F. Ferreira, et al., Antibacterial naphthoquinone derivatives targeting resistant strain Gram-negative bacteria in biofilms, Microb. Pathog. 118 (2018) 105–114, https://doi.org/10.1016/j.micpath.2018.03.024.

[19] G.C. Brandão, F.C. Rocha Missias, L.M. Arantes, L.F. Soares, K.K. Roy, R.J. Doerksen, et al., Antimalarial naphthoquinones. Synthesis via click chemistry, *in vitro* activity, docking to PfDHODH and SAR of lapachol-based compounds, Eur. J. Med. Chem. 145 (2018) 191–205, https://doi.org/10.1016/j.ejmech.2017.12.051.

[20] E.C.B. Da Costa, R. Amorim, F.C. Da Silva, D.R. Rocha, M.P. Papa, L.B. De Arruda, et al., Synthetic 1,4-pyran naphthoquinones are potent inhibitors of dengue virus replication, PLoS One 8 (2013) 1–11, https://doi.org/10.1371/journal.pone.0082504.

[21] V. Prachayasittikul, R. Pingaew, A. Worachartcheewan, C. Nantasenamat, S. Prachayasittikul, S. Ruchirawat, et al., Synthesis, anticancer activity and QSAR study of 1,4-naphthoquinone derivatives, Eur. J. Med. Chem. 84 (2014) 247–263, https://doi.org/10.1016/j.ejmech.2014.07.024.

[22] R. Verma, Anti-cancer activities of 1,4-naphthoquinones: a QSAR Study, Anticancer. Agents Med. Chem. 6 (2006) 489–499, https://doi.org/10.2174/187152006778226512.

[23] J. Benites, J.A. Valderrama, K. Bettega, R.C. Pedrosa, P.B. Calderon, J. Verrax, Biological evaluation of donor-acceptor aminonaphthoquinones as antitumor agents, Eur. J. Med. Chem. 45 (2010) 6052–6057, https://doi.org/10.1016/j.ejmech.2010.10.006.

[24] L.I. López-López, D.S. Nery-Flores, Y.S. Silva-Belmares, A. Sáenz-Galindo, Naphthoquinones: Biological properties and synthesis of lawsone and derivatives - a structured review, Vitae 21 (2014) 248–258.

[25] D.K. Singh, S. Luqman, Lawsonia inermis (L.): a perspective on anticancer potential of Mehndi/Henna, Biomed. Res. Ther. 1 (2014) 112–120, https://doi.org/10.7603/s40730-014-0018-1.

[26] E. Coelho-Cerqueira, P.A. Netz, V.P. Do Canto, A.C. Pinto, C. Follmer, Beyond topoisomerase inhibition: antitumor 1,4-naphthoquinones as potential inhibitors of human monoamine oxidase, Chem. Biol. Drug Des. 83 (2014) 401–410, https://doi.org/10.1111/cbdd.12255.

[27] S. Oramas-Royo, C. Torrejón, I. Cuadrado, R. Hernández-Molina, S. Hortelano, A. Estévez-Braun, et al., Synthesis and cytotoxic activity of metallic complexes of lawsone, Bioorganic Med. Chem. 21 (2013) 2471–2477, https://doi.org/10.1016/j.bmc.2013.03.002.

[28] K.M. Oliveira, L. Liany, R.S. Corrêa, V.M. De, M.R. Cominetti, A.A. Batista, Selective Ru (II)/lawsone complexes inhibiting tumor cell growth by apoptosis, J. Inorg. Biochem. 176 (2017) 66–76, https://doi.org/10.1016/j.jinorgbio.2017.08.019.

[29] T.A. Heinrich, G. Von Poelhsitz, R.I. Reis, E.E. Castellano, A. Neves, M. Lanznaster, et al., A new nitrosyl ruthenium complex: synthesis, chemical characterization, *in vitro* and *in vivo* antitumor activities and probable mechanism of action, Eur. J. Med. Chem. 46 (2011) 3616–3622, https://doi.org/10.1016/j.ejmech.2011.04.064.

[30] R.A. De Grandis, M.S. de Camargo, M.M. da Silva, É.O. Lopes, E.C. Padilha, F.A. Resende, et al., Human topoisomerase inhibition and DNA/BSA binding of Ru (II)–SCAR complexes as potential anticancer candidates for oral application, BioMetals 30 (2017) 321–334, https://doi.org/10.1007/s10534-017-0008-z.

[31] K.M. Oliveira, R.S. Corrêa, M.I.F. Barbosa, J. Ellena, M.R. Cominetti, A.A. Batista, Ruthenium (II)/triphenylphosphine complexes: an effective way to improve the cytotoxicity of lapachol, Polyhedron 130 (2017) 108–114, https://doi.org/10.1016/j.poly.2017.04.005.

[32] L. Colina-Vegas, J.L. Dutra, W. Villarreal, J.H. João, M.R. Cominetti, F. Pavan, et al., Ru(II)/clotrimazole/diphenylphosphine/bipyridine complexes: Interaction with DNA, BSA and biological potential against tumor cell lines and *Mycobacterium tuberculosis*, J. Inorg. Biochem. 162 (2016) 135–145, https://doi.org/10.1016/j.jinorgbio.2016.06.023.

[33] M.S. de Camargo, M.M. da Silva, R.S. Correa, S.D. Vieira, S. Castelli, I. D'Anessa, et al., Inhibition of human DNA topoisomerase IB by nonmutagenic ruthenium(II)-based compounds with antitumoral activity, Metallomics 8 (2016) 179–192, https://doi.org/10.1039/C5MT00227C.

[34] N.C. De Carvalho, S.P. Neves, R.B. Dias, L.D.F. Valverde, C.B.S. Sales, C.A.G. Rocha, et al., A novel ruthenium complex with xanthoxylin induces S-phase arrest and causes ERK1/2-mediated apoptosis in HepG2 cells through a p53-independent pathway article, Cell Death Dis. 9 (2018), https://doi.org/10.1038/s41419-017-0104-6.

[35] W.C. Pires, B.A.V. Lima, F. de Castro Pereira, A.P. Lima, F. Mello-Andrade, H.D. Silva, et al., Ru(II)/diphenylphosphine/pyridine-6-thiolate complexes induce S-180 cell apoptosis through intrinsic mitochondrial pathway involving inhibition of Bcl-2 and p53/Bax activation, Mol. Cell. Biochem. 438 (2018) 199–217, https://doi.org/10.1007/s11010-017-3129-3.

[36] E. Rutkowska, K. Pająk, K. Jóźwiak, Lipophilicity - Methods of determination and its role in medicinal chemistry, Acta Pol. Pharm. Drug Res. 70 (2013) 3–18.

[37] O. Guideline, for testing os chemicals, Partition coefficient (*n*-octanol/water): shake flask method, OECD Guidel. 107 (1995) 1–4, https://doi.org/10.1787/9789264069626-en.

[38] D.F. Segura, A.V.G. Netto, R.C.G. Frem, A.E. Mauro, P.B. Da Silva, J.A. Fernandes, et al., Synthesis and biological evaluation of ternary silver compounds bearing N, N-chelating ligands and thiourea: X-ray structure of [{Ag(bpy)(μ-tu)$_3$2](N$_O$3)2(bpy = 2,2′-bipyridine; Tu = thiourea), Polyhedron 79 (2014) 197–206, https://doi.org/10.1016/j.poly.2014.05.004.

[39] C.J. Lima, L. Rodríguez, Phosphine-gold (I) compounds as anticancer agents: general description and mechanisms of action, Anticancer. Agents Med. Chem. 11 (2011) 921–928.

[40] W. Villarreal, L. Colina-Vegas, G. Visbal, O. Corona, R.S. Corrêa, J. Ellena, et al., Copper(I)-phosphine polypyridyl complexes: synthesis, characterization, DNA/HSA binding study, and antiproliferative activity, Inorg. Chem. 56 (2017) 3781–3793, https://doi.org/10.1021/acs.inorgchem.6b02419.

[41] J.J. Liu, P. Galettis, A. Farr, L. Maharaj, H. Samarasinha, A.C. McGechan, et al., *In vitro* antitumour and hepatotoxicity profiles of Au(I) and Ag(I) bidentate pyridyl phosphine complexes and relationships to cellular uptake, J. Inorg. Biochem. 102 (2008) 303–310, https://doi.org/10.1016/j.jinorgbio.2007.09.003.

[42] L. Biancalana, S. Zacchini, N. Ferri, M.G. Lupo, G. Pampaloni, F. Marchetti, Tuning the cytotoxicity of ruthenium(II) para-cymene complexes by mono-substitution at a triphenylphosphine/phenoxydiphenylphosphine ligand, Dalt. Trans. 46 (2017) 16589–16604, https://doi.org/10.1039/C7DT03385K.

[43] N.A.P. Franken, H.M. Rodermond, J. Stap, J. Haveman, C. van Bree, Clonogenic assay of cells in vitro, Nat. Protoc. 1 (2006) 2315–2319, https://doi.org/10.1038/nprot.2006.339.

[44] L. Galluzzi, S.A. Aaronson, J. Abrams, E.S. Alnemri, D.W. Andrews, E.H. Baehrecke, et al., Guidelines for the use and interpretation of assays for monitoring cell death in higher eukaryotes, Cell Death Differ. 16 (2009) 1093–1107, https://doi.org/10.1038/cdd.2009.44.

[45] L.C. Kimlin, G. Casagrande, V.M. Virador, *In vitro* three-dimensional (3D) models in cancer research: an update, Mol. Carcinog. 52 (2013) 167–182, https://doi.org/10.1002/mc.21844.

[46] S.A. Langhans, Three-dimensional *in vitro* cell culture models in drug discovery and drug repositioning, Front. Pharmacol. 9 (2018) 1–14, https://doi.org/10.3389/fphar.2018.00006.

[47] W.N. Hait, Anticancer drug development: the grand challenges, Nat. Rev. Drug Discov. 9 (2010) 253–254, https://doi.org/10.1038/nrd3144.

[48] E.T.9.J. Doijen, W. Luyten, B. Landuyt, L. Schoofs, Three-dimensional cell culture models for anticancer drug screening: Worth the effort? J. Cell. Physiol. (2017) 2993–3003, https://doi.org/10.1002/jcp.26052.

[49] G. Mehta, A.Y. Hsiao, M. Ingram, G.D. Luker, S. Takayama, Opportunities and challenges for use of tumor spheroids as models to test drug delivery and efficacy, J. Control. Release. 164 (2012) 192–204, https://doi.org/10.1016/j.jconrel.2012.04.045.

[50] P. Parhi, S. Suklabaidya, S.K. Sahoo, Enhanced anti-metastatic and anti-tumorigenic efficacy of Berbamine loaded lipid nanoparticles *in vivo*, Sci. Rep. (2017) 1–13, https://doi.org/10.1038/s41598-017-05296-y.

[51] L.F. Magalhães, F. Mello-Andrade, W.C. Pires, H.D. Silva, P.F.F. da Silva, L.M. Macedo, et al., *cis*-[RuCl(BzCN)(bipy)(dppe)]PF_6 induces anti-angiogenesis and apoptosis by a mechanism of caspase-dependent involving DNA damage, PARP activation, and Tp53 induction in Ehrlich tumor cells, Chem. Biol. Interact. 278 (2017) 101–113, https://doi.org/10.1016/j.cbi.2017.09.013.

[52] P. Lu, V.M. Weaver, Z. Werb, The extracellular matrix: A dynamic niche in cancer progression, J. Cell Biol. 196 (2012) 395–406, https://doi.org/10.1083/jcb.201102147.

[53] A. Vacca, M. Bruno, A. Boccarelli, M. Coluccia, D. Ribatti, A. Bergamo, et al., Inhibition of endothelial cell functions and of angiogenesis by the metastasis inhibitor NAMI-A, Br. J. Cancer. 4 (2002) 993–998, https://doi.org/10.1038/sj/bjc/6600176.

[54] L. Gu, X. Li, Q. Ran, C. Kang, C. Lee, J. Shen, Antimetastatic activity of novel ruthenium (III) pyridine complexes, Cancer Med. 5 (2016) 2850–2860, https://doi.org/10.1002/cam4.826.

[55] G. Barone, A. Terenzi, A. Lauria, A.M. Almerico, J.M. Leal, N. Busto, et al., DNA-binding of nickel(II), copper(II) and zinc(II) complexes: structure-affinity relationships, Coord. Chem. Rev. 257 (2013) 2848–2862, https://doi.org/10.1016/j.ccr.2013.02.023.

[56] N. Narayanaswamy, M. Kumar, S. Das, R. Sharma, P.K. Samanta, S.K. Pati, et al., A thiazole coumarin (TC) turn-on fluorescence probe for AT-base pair detection and multipurpose applications in different biological systems, Sci. Rep. 4 (2014) 1–10, https://doi.org/10.1038/srep06476.

[57] T. Sarwar, M.A. Husain, S.U. Rehman, H.M. Ishqi, M. Tabish, Multi-spectroscopic and molecular modelling studies on the interaction of esculetin with calf thymus DNA, Mol. Biosyst. 11 (2015) 522–531, https://doi.org/10.1039/c4mb00636d.

[58] D. Hanahan, R. Weinberg, The hallmarks of cancer, Cell 100 (2000) 57–70, https://doi.org/10.1007/s00262-010-0968-0.

[59] D. Hanahan, R. Weinberg, Hallmarks of cancer: the next generation, Cell 144 (2011) 646–674, https://doi.org/10.1016/j.cell.2011.02.013.

[60] I. Vermes, C. Haanen, H. Steffens-Nakken, C. Reutelingsperger, A novel assay for apoptosis Flow cytometric detection of phosphatidylserine early apoptotic cells using fluorescein labelled expression on Annexin V, J. Immunol. Methods 184 (1995) 39–51.

[61] F. Mello-Andrade, W.L. da Costa, W.C. Pires, F.de.C. Pereira, C.G. Cardoso, R.de.S. Lino-Junior, et al., Antitumor effectiveness and mechanism of action of Ru (II)/amino acid/diphosphine complexes in the peritoneal carcinomatosis progression, Tumor Biol. 39 (2017) 1–18, https://doi.org/10.1177/1010428317695933.

[62] Z. Deng, P. Gao, L. Yu, B. Ma, Y. You, L. Chan, et al., Ruthenium complexes with phenylterpyridine derivatives target cell membrane and trigger death receptors-mediated apoptosis in cancer cells, Biomaterials 129 (2017) 111–126, https://doi.org/10.1016/j.biomaterials.2017.03.017.

[63] H. Perlman, X. Zhang, M.W. Chen, K. Walsh, R. Buttyan, An elevated *BAX/BCL-2* ratio corresponds with the onset of prostate epithelial cell apoptosis, Cell Death Differ. 6 (1999) 48–54, https://doi.org/10.1038/sj.cdd.4400453.

[64] R. Kasiappan, S. Safe, ROS-inducing agents for cancer chemotherapy, React. Oxyg. Species 1 (2016) 22–37, https://doi.org/10.20455/ros.2016.805.

[65] K.W. Wellington, Understanding cancer and the anticancer activities of naphthoquinones – a review, RSC Adv. 5 (2015) 20309–20338, https://doi.org/10.1039/C4RA13547D.

[66] M. Halasi, M. Wang, T.S. Chavan, V. Gaponenko, N. Hay, A.L. Gartel, ROS inhibitor *N* -acetyl-L-cysteine antagonizes the activity of proteasome inhibitors, Biochem. J. 454 (2013) 201–208, https://doi.org/10.1042/BJ20130282.

[67] L.O. Klotz, X. Hou, C. Jacob, 1,4-naphthoquinones: From oxidative damage to cellular and inter-cellular signaling, Molecules 19 (2014) 14902–14918, https://doi.org/10.3390/molecules190914902.

[68] A. Bergamo, G. Sava, Linking the future of anticancer metal-complexes to the therapy of tumour metastases, Chem. Soc. Rev. 44 (2015) 8818–8835, https://doi.org/10.1039/C5CS00134J.

[69] J.X. Liang, H.J. Zhong, G. Yang, K. Vellaisamy, D.L. Ma, C.H. Leung, Recent development of transition metal complexes with *in vivo* antitumor activity, J. Inorg. Biochem. 177 (2017) 276–286, https://doi.org/10.1016/j.jinorgbio.2017.06.002.

[70] W.M. Motswainyana, P.A. Ajibade, Anticancer activities of mononuclear ruthenium (II) coordination complexes, Adv. Chem. 2015 (2015) 1–21, https://doi.org/10.1155/2015/859730.

[71] A.M. Al-Majid, S. Yousuf, M.I. Choudhary, F. Nahra, S.P. Nolan, Gold-NHC complexes as potent bioactive compounds, ChemistrySelect 1 (2016) 76–80, https://doi.org/10.1002/slct.201600009.

[72] M. Porchia, F. Tisato, M. Zancato, V. Gandin, C. Marzano, *In vitro* antitumor activity of water-soluble copper(I) complexes with diimine and monodentate phosphine ligands, Arab. J. Chem. (2017), https://doi.org/10.1016/j.arabjc.2017.09.003.

[73] M. Echeverri, A. Alvarez-Valdés, F. Navas, J. Perles, I. Sánchez-Pérez, A.G. Quiroga, Using phosphine ligands with a biological role to modulate reactivity in novel platinum complexes, R. Soc. Open Sci. 5 (2018), https://doi.org/10.1098/rsos.171340.

[74] M.J. McKeage, S.J. Berners-Price, P. Galettis, R.J. Bowen, W. Brouwer, L. Ding, et al., Role of lipophilicity in determining cellular uptake and antitumour activity of gold phosphine complexes, Cancer Chemother. Pharmacol. 46 (2000) 343–350, https://doi.org/10.1007/s002800000166.

[75] A. Bal-Price, S. Coecke, Guidance on good cell culture practice (GCCP), Cell Cult Tech. (2011) 1–25, https://doi.org/10.1007/978-1-61779-077-5_1.

[76] B.P. Sullivan, D.J. Salmon, T.J. Meyer, Mixed phosphine 2,2'-bipyridine complexes of ruthenium, Inorg. Chem. 17 (1978) 3334–3341, https://doi.org/10.1021/ic50190a006.

[77] A.A. Batista, M.O. Santiago, C.L. Donnici, I.S. Moreira, P.C. Healy, S.J. Berners-Price, et al., Electrochemical and spectroscopic studies on RuCl2(PPh3)2(N)2 and RuCl2(PPh3)2(N–N) complexes (N = pyridine derivatives and N-N = phenanthroline or bipyridine derivatives). X-ray structure of RuCl2(PPh3)2(phen), Polyhedron 20 (2001) 2123–2128, https://doi.org/10.1016/S0277-5387(01)00744-6.

[78] E. Baka, J.E.A. Comer, K. Takács-Novák, Study of equilibrium solubility measurement by saturation shake-flask method using hydrochlorothiazide as model compound, J. Pharm. Biomed. Anal. 46 (2008) 335–341, https://doi.org/10.1016/j.jpba.2007.10.030.

[79] S. Page, Ruthenium compounds as anticancer agents, Educ. Chem. 26–29 (2012).

[80] J. Friedrich, C. Seidel, R. Ebner, L.A. Kunz-Schughart, Spheroid-based drug screen: considerations and practical approach, Nat. Protoc. 4 (2009) 309–324, https://doi.org/10.1038/nprot.2008.226.

[81] J. Marmur, A procedure for the isolation of deoxyribonucleic acid from micro-organisms, J. Mol. Biol. 3 (1961) IN1-218, https://doi.org/10.1016/S0022-2836(61)80047-8.

[82] B.S. Cummings, L.P. Wills, R.G. Schnellmann, Measurement of cell death in mammalian cells, Curr. Protoc. Phamacol. 1 (2004) 1–30, https://doi.org/10.1002/0471141755.ph1208s25.

[83] T.D. Schmittgen, K.J. Livak, Analyzing real-time PCR data by the comparative C(T) method, Nat. Protoc. 3 (2008) 1101–1108, https://doi.org/10.1038/nprot.2008.73.

[84] H. Wang, J.A. Joseph, Quantifying cellular oxidative stress by dichlorofluorescein assay using microplate reader, Free Radic. Biol. Med. 27 (1999) 612–616, https://doi.org/10.1016/S0891-5849(99)00107-0.